ARL

The Feasibility of Radio Direction Finding for Swarm Localization

by Michael L Don

NOTICES

Disclaimers

US Army Research Laboratory

The Feasibility of Radio Direction Finding for Swarm Localization

by Michael L Don
Weapons and Materials Research Directorate, ARL

REPORT DOCUMENTATION PAGE

Public reporting burden for this collection of information is estimated to average 1 hour per response, including the time for reviewing instructions, searching existing data sources, gathering and maintaining the data needed, and completing and reviewing the collection information. Send comments regarding this burden estimate or any other aspect of this collection of information, including suggestions for reducing the burden, to Department of Defense, Washington Headquarters Services, Directorate for Information Operations and Reports (0704-0188), 1215 Jefferson Davis Highway, Suite 1204, Arlington, VA 22202-4302. Respondents should be aware that notwithstanding any other provision of law, no person shall be subject to any penalty for failing to comply with a collection of information if it does not display a currently valid OMB control number.
PLEASE DO NOT RETURN YOUR FORM TO THE ABOVE ADDRESS.

1. REPORT DATE *(DD-MM-YYYY)*	2. REPORT TYPE	3. DATES COVERED (From - To)
September 2017	Technical Report	February 1 2017–August 1 2017

4. TITLE AND SUBTITLE	5a. CONTRACT NUMBER
The Feasibility of Radio Direction Finding for Swarm Localization	
	5b. GRANT NUMBER
	5c. PROGRAM ELEMENT NUMBER
6. AUTHOR(S)	5d. PROJECT NUMBER
Michael L Don	6
	5e. TASK NUMBER
	5f. WORK UNIT NUMBER

7. PERFORMING ORGANIZATION NAME(S) AND ADDRESS(ES)	8. PERFORMING ORGANIZATION REPORT NUMBER
US Army Research Laboratory Weapons and Materials Research Directorate (ATTN: RDRL-WML-F) Aberdeen Proving Ground, MD 21005-5066	ARL-TR-8114

9. SPONSORING/MONITORING AGENCY NAME(S) AND ADDRESS(ES)	10. SPONSOR/MONITOR'S ACRONYM(S)
	11. SPONSOR/MONITOR'S REPORT NUMBER(S)

12. DISTRIBUTION/AVAILABILITY STATEMENT
Approved for public release; distribution is unlimited.

13. SUPPLEMENTARY NOTES

14. ABSTRACT
The US Army Research Laboratory (ARL) is investigating technologies to assist in swarm localization. One promising technology is radio direction finding (RDF). RDF has been used since World War I and has many applications both in the military and private sectors, but compact commercial systems suitable for deployment on small swarm agents do not exist. This has led ARL to begin development of a custom RDF system using small, standalone, software-defined radios (SDRs). First, basic RDF theory is presented. Next, a laboratory experiment to evaluate RDF using a SDR is developed. Finally, experimental data are presented supporting the feasibility of RDF for swarm localization.

15. SUBJECT TERMS
radio direction finding, angle of arrival, direction of arrival, localization, swarm, software-defined radio

16. SECURITY CLASSIFICATION OF:			17. LIMITATION OF ABSTRACT	18. NUMBER OF PAGES	19a. NAME OF RESPONSIBLE PERSON
a. REPORT	b. ABSTRACT	c. THIS PAGE	UU	52	Michael L Don
					19b. TELEPHONE NUMBER (Include area code)
Unclassified	Unclassified	Unclassified			410-306-0775

Contents

List of Figures

List of Tables

Acknowledgments

I would like to acknowledge Rex Hall from the US Army Research Laboratory and Jonathan Hallameyer from Bowhead for their help with the experiment setup in the antenna chamber.

1.   Introduction

The US Army Research Laboratory (ARL) is investigating the advantages of group swarming behavior over a comparable group of solitary agents. One advantage is the ability for swarm agents to localize relative to the group using spatial relationships between many agents to achieve accurate relative attitude and position information.[1] This is particularly important in GPS-denied environments where there are limited options for absolute positioning.[2] In these cases, it is possible for a swarm with relative positioning to use one agent with absolute localization to grant absolute localization to the entire swarm. Applications also exist for relative positioning alone, such as collision avoidance,[3] formation flying,[4] and patterned weapon delivery.[5]

One method to achieve relative localization is radio direction finding (RDF). There are several ways to perform RDF, but commonly the phase differences between the elements of an antenna array are used to determine a radio signal's angle of arrival (AoA).[6] An agent can then determine its relative attitude and position using known angles to the other swarm agents. RDF has been used since World War I[7] and has many applications such as ship and aircraft navigation, search and rescue, wildlife tracking, location of illegal radio transmissions, missile guidance, radar systems, and antiradiation missiles.[8]

Despite RDF's long history and many successful applications, a suitable commercial off-the-shelf device for swarms of small agents does not exist. Larger systems for search and rescue[9] and radar cannot be easily adapted to small swarm agents, while smaller automotive radar systems have limited range.[10] Instead of using the phase interferometry approach, many systems use time difference of arrival or received-signal-strength-indication methods that do not achieve high accuracy.[11] Phase interferometry using antenna arrays can be difficult to implement because antenna characteristics and multipath effects can significantly degrade performance. Despite these problems, literature suggests that a reliable RDF system could be designed for swarm-relative localization.[12] There are 2 significant reasons why many swarm applications present fewer design challenges than other RDF applications. First, high-altitude swarms, such as swarms of unmanned aerial vehicles (UAVs) or munitions, will not be significantly affected by multipath. Secondly, many swarms can have antenna arrays attached to the agents in a repeatable manner, simplifying antenna characterization issues. Compare this with a device such as a cell phone, whose possible orientation and proximity to other objects makes assumptions about antenna performance problematic.

This report shows the feasibility of RDF for swarm-relative localization by demonstrating RDF with a simple 2-element antenna array with a small standalone software-defined radio (SDR). First, the theory of phase-interferometry RDF is presented. Next, an RDF system is described and simulated, including the practical considerations of the radio receiver. The software design and hardware setup of an RDF laboratory experiment is explained next, followed by the experimental results. Finally, the results are summarized and future research directions are explored.

2. Phase-Interferometry Radio Direction Finding

The AoA of an RF signal can be determined using the system in Fig. 1. A_1 and A_2 indicate the position of 2 antennas spaced a distance d apart. The red lines indicate the RF signal's direction of propagation from the source to the antennas. If the distance from the signal source to the antennas is much greater than d, these lines can be assumed to be parallel. The AoA, θ, is shown as the angle off-center of the incoming RF signal that intersects A_2. Since $\theta + \alpha = 90°$ and $\theta + \angle PA_1A_2 = 90°$, then $\angle PA_1A_2$ is also θ. The length of $\overline{PA_2}$ is the difference in distance that the RF signal must travel to A_2 as compared with A_1. Given an RF signal with wavelength λ, assuming $d \leq \lambda/2$ and $-90° \leq \theta \leq 90°$, the phase difference between the received signals at A_1 and A_2 is given by

$$\Delta\phi = 2\pi \left(\frac{d \sin\theta}{\lambda} \right), \tag{1}$$

where $-\pi \leq \Delta\phi \leq \pi$. Here and in the rest of the report, phases are in radians, while angles are in degrees. Given a measured phase difference between A_1 and A_2, the angle of arrive is then

$$\theta = \sin^{-1}\left(\frac{\lambda\left(\frac{\Delta\phi}{2\pi}\right)}{d} \right). \tag{2}$$
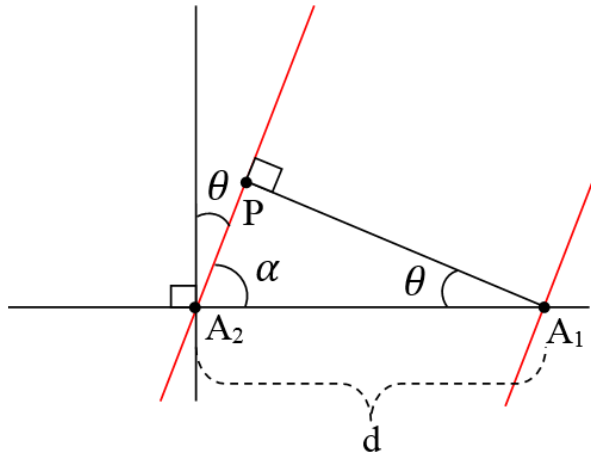

Fig. 1   AoA system with 2 antennas

From Eq. 1, if $d > \lambda/2$, $\Delta\phi$ can exceed the range of $-\pi \leq \Delta\phi \leq \pi$. This causes an ambiguity problem since values of $\Delta\phi$ and $\Delta\phi \pm 2\pi$ cannot be distinguished from each other at the antennas, leading to multiple solutions for θ. To correct this problem, an integer I can be added to Eq. 2 to account for the phase roll-overs:

$$\theta = \sin^{-1}\left(\frac{\lambda\left(\frac{\Delta\phi}{2\pi}+I\right)}{d}\right). \tag{3}$$

For a range of $-\theta_{max} \leq \theta \leq \theta_{max}$, the maximum distance of $\overline{PA_2}$ is $\pm d \sin\theta_{max}$. Examining increasing values of θ, the first-phase roll-over will occur when $\Delta\phi = \pi$, corresponding to $\overline{PA_2} = \lambda/2$. Each additional roll-over will occur at an additional phase change of 2π, corresponding to additional multiples of λ in length $\overline{PA_2}$. Therefore, for a range of $-\theta_{max} \leq \theta \leq \theta_{max}$, the range of I will be $-I_{max} \leq I \leq I_{max}$, with I_{max} given as

$$I_{max} = \left\lfloor \frac{d \sin\theta_{max} + \lambda/2}{\lambda} \right\rfloor, \tag{4}$$

with $\lfloor x \rfloor$ indicating the floor of x. A typical method to determine I is to use 3 antennas, with distances d_{12} and d_{13} denoting the spacing between the first and second and first and third antennas, respectively, leading to 2 phase measurements, $\Delta\phi_{12}$ and $\Delta\phi_{13}$.[13] Rearranging Eq. 3 for each pair of antennas gives

$$\Delta\phi_{12} - 2\pi I_{12} = 2\pi\left(\frac{d_{12}\sin\theta}{\lambda}\right) \tag{5}$$

and

$$\Delta\phi_{13} - 2\pi I_{13} = 2\pi\left(\frac{d_{13}\sin\theta}{\lambda}\right). \tag{6}$$

Solving for $\Delta\phi_{13}$ in terms of $\Delta\phi_{12}$ gives

$$\Delta\phi_{13} = \frac{d_{13}}{d_{12}}\Delta\phi_{12} - \frac{d_{13}}{d_{12}}2\pi I_{12} + 2\pi I_{13}. \tag{7}$$

In many AoA applications, the direction finding system has no control over the signal being detected, but in applications where one has control over the transmitted signal, an alternative way of resolving the ambiguity presents itself. Instead of using 2 different antenna spacings, 2 different transmit frequencies can be used. Equations 5 and 6 now become

$$\Delta\phi_1 - 2\pi I_1 = 2\pi\left(\frac{d\sin\theta}{\lambda_1}\right) \tag{8}$$

and

$$\Delta\phi_2 - 2\pi I_2 = 2\pi\left(\frac{d\sin\theta}{\lambda_2}\right), \tag{9}$$

and Eq. 7 becomes

$$\Delta\phi_2 = \frac{\lambda_1}{\lambda_2}\Delta\phi_1 - \frac{\lambda_1}{\lambda_2}2\pi I_1 + 2\pi I_2. \tag{10}$$

Equation 10 indicates a linear relationship between the phase measurements $\Delta\phi_1$ and $\Delta\phi_2$ for each possible combination of I_1 and I_2, which will be referred to as phase lines. An example scenario showing values of $\Delta\phi_1$ and $\Delta\phi_2$ for $-80° \leq \theta \leq 80°$ is shown in Fig. 2 for $d = 26.6$ cm, $\lambda_1 = 12.5$ cm, and $\lambda_2 = 15.625$ cm. In this case, both I_1 and I_2 are in the range $-2 < I_1, I_2 < 2$ for $-80° \leq \theta \leq 80°$, resulting in the phase lines shown in Fig. 3. A total of 100 phase measurements from Fig. 2 are plotted as $(\Delta\phi_1, \Delta\phi_2)$ phase points that occur on their respective phase lines. The line of a phase point determines its values of I_1 and I_2, which can then be inserted into Eqs. 8 and 9 to unwrap the phase measurements and determine an unambiguous value for θ. Figure 4 shows this process by displaying the original phase measurements, the correction factor of $-2\pi I$ from Eqs. 8 and 9, and the unwrapped phases for both λ_1 and λ_2 found by adding the correction factor to the phase measurements.
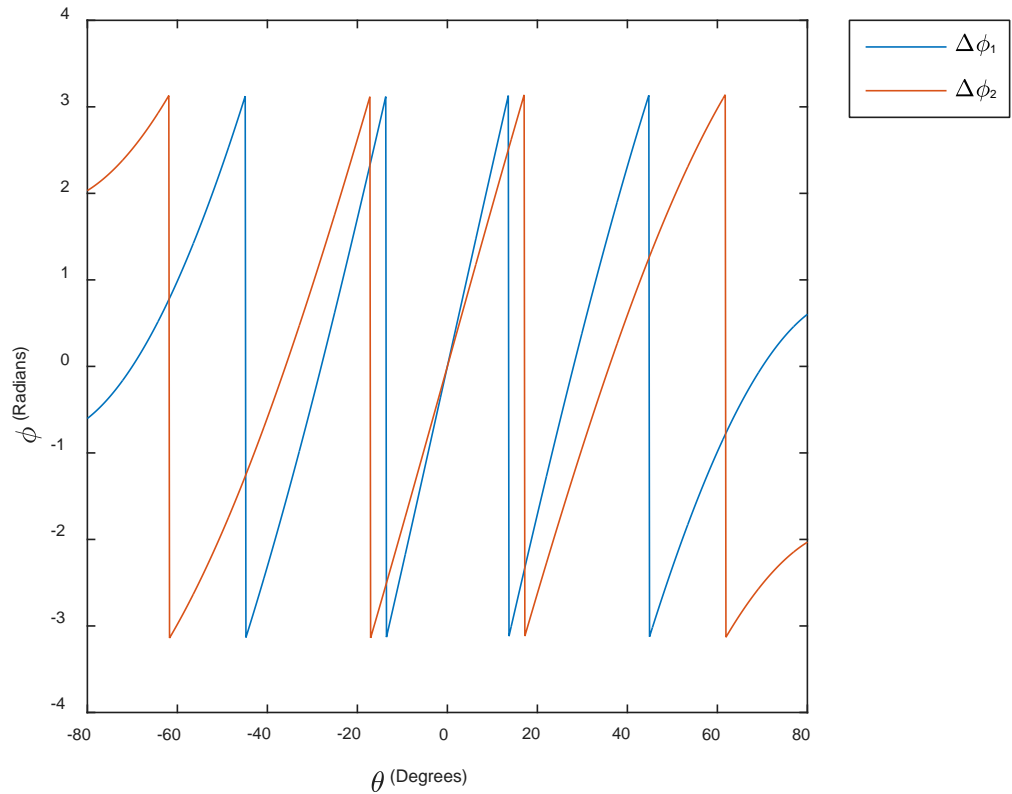

Fig. 2   Example phase measurements for 2 wavelengths
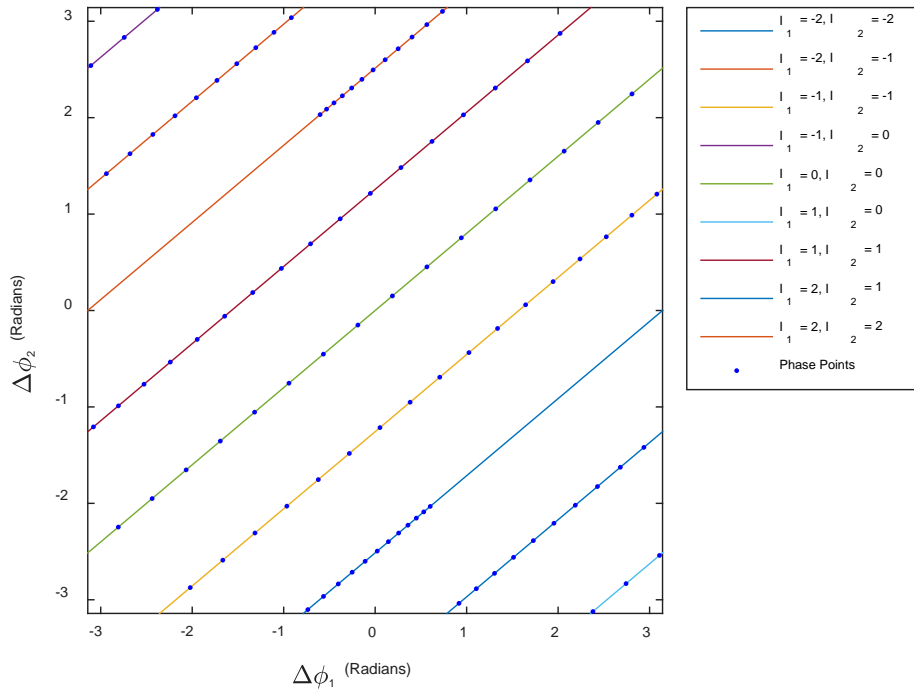
Fig. 3   Example phase line plot with phase points
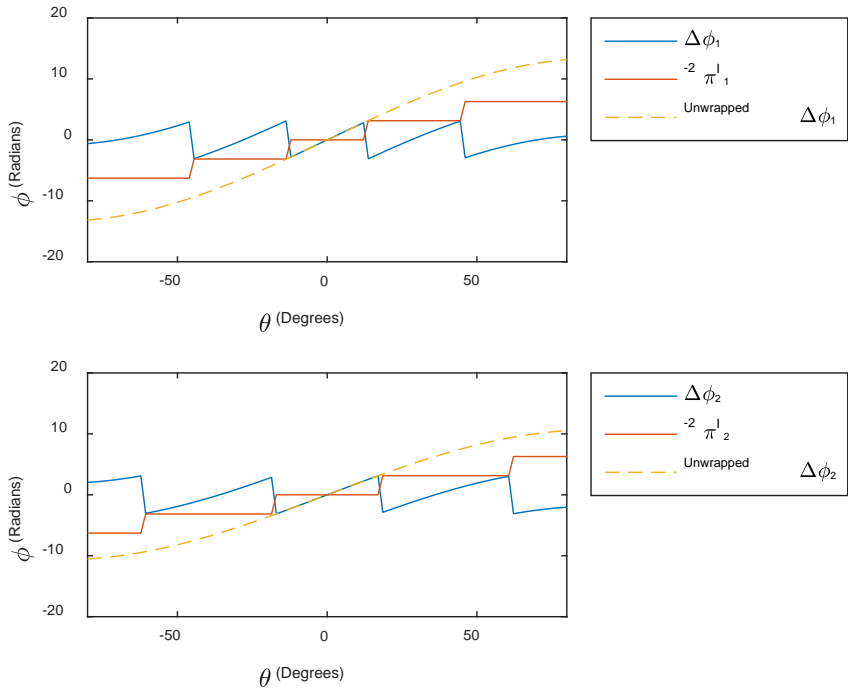
Fig. 4   Unwrapping phase measurements for the first wavelength (top) and second wavelength (bottom)

This example showed an ideal case with perfect measurements. Figures 5–8 show the same example with $\mathcal{N}(0,0.025)$ Gaussian noise added to the $\Delta\phi$ measurements. In Fig. 6 the phase points $(\Delta\phi_1, \Delta\phi_2)$ no longer lie directly on the phase lines. This means that we can no longer directly determine the values of I_1 and I_2 by solving Eq. 10 (i.e., matching the phase point to its respective phase line). Instead, the phase line closest to the phase point is used to determine its values of I_1 and I_2. The distance δ from point $(\Delta\phi_1, \Delta\phi_2)$ to the phase lines in Eq. 10 is

$$\delta = \frac{\left|\Delta\phi_2 - \frac{\lambda_1}{\lambda_2}\Delta\phi_1 + \frac{\lambda_1}{\lambda_2}2\pi I_1 - 2\pi I_2\right|}{\sqrt{\left(\frac{\lambda_1}{\lambda_2}\right)^2 + 1}}. \tag{11}$$

Using δ to determine the most-likely values of I_1 and I_2 for each phase point, Fig. 7 shows the correction factor of $-2\pi I$ and the unwrapped phases for λ_1 and λ_2 measurements with the final angle calculations and angle error displayed in Fig. 8. The angle error increases with θ because for larger angles a small change in phase corresponds to a large change in θ.
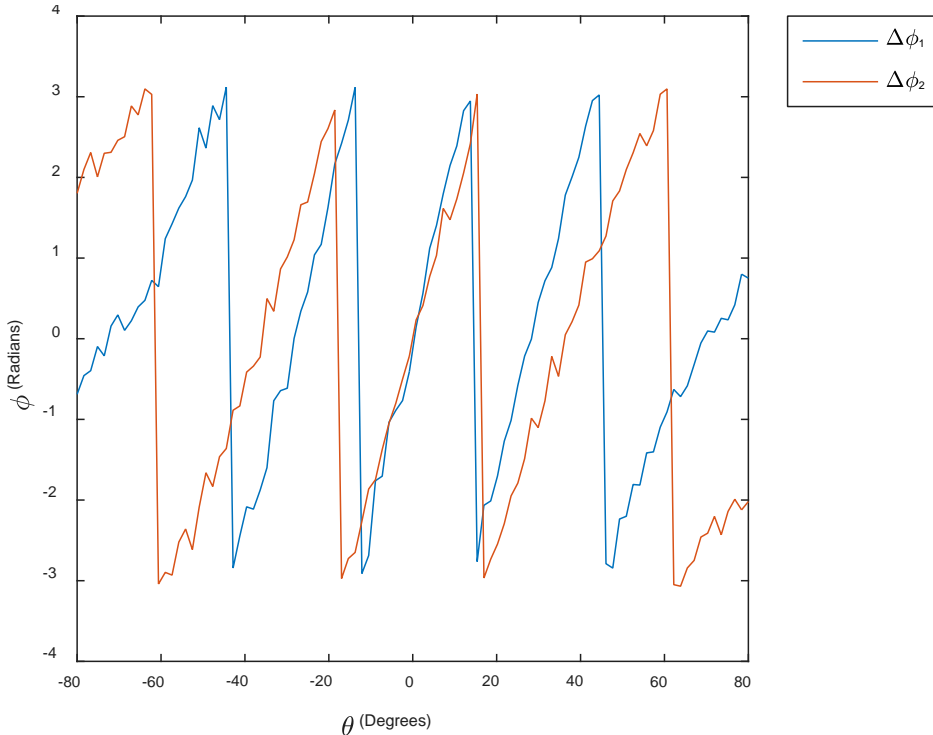
**Fig. 5**   **Noisy phase measurements for 2 wavelengths**
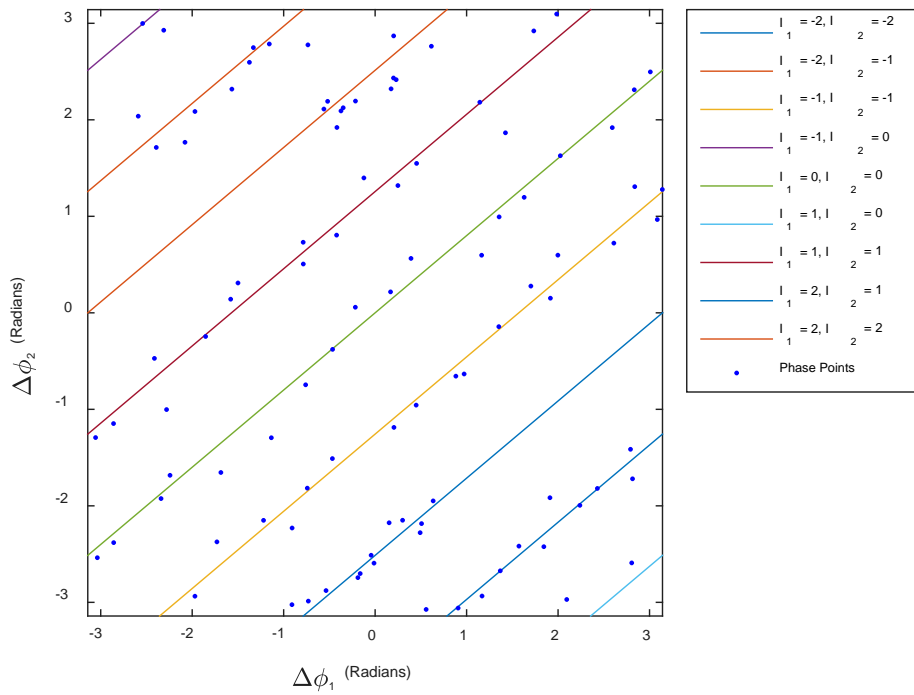
**Fig. 6   Phase lines with noisy phase points**
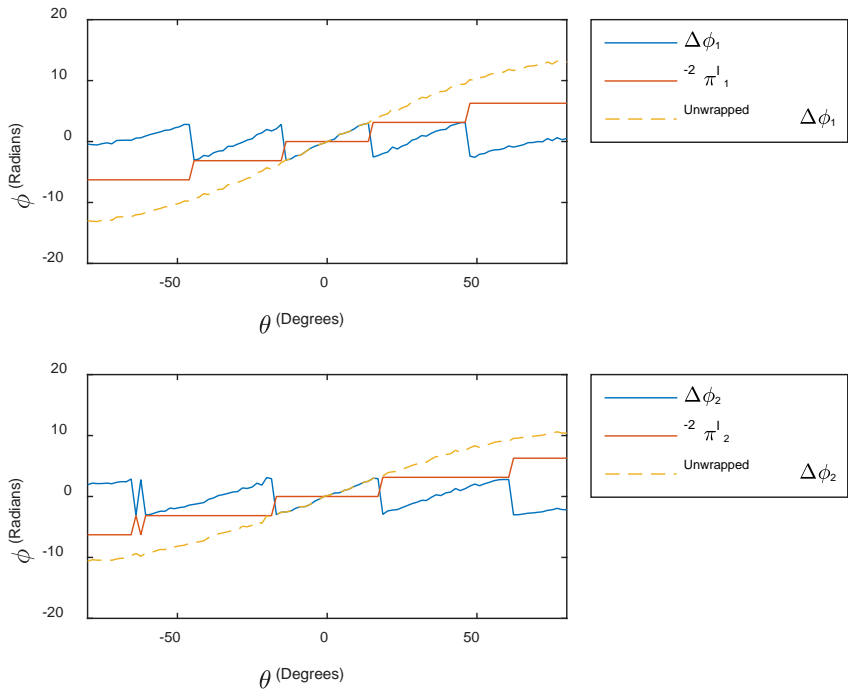
Fig. 7   Unwrapping noisy phase measurements for the first wavelength (top) and second wavelength (bottom)
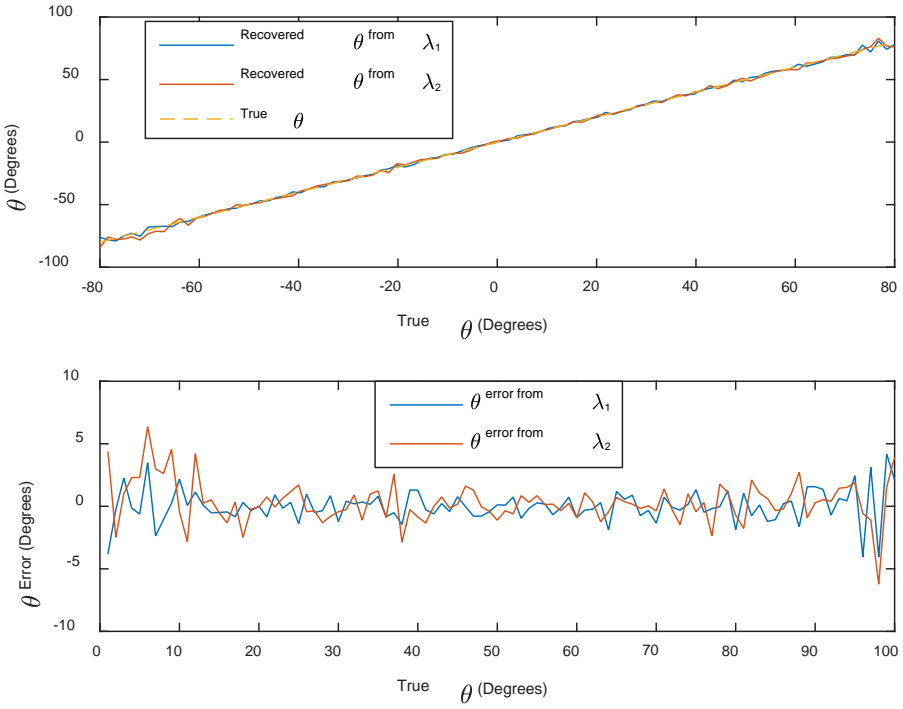
Fig. 8   Recovered angle vs. the true angle (top) and the recovered angle error (bottom) for noisy phase measurements

As the level of noise increases, phase points may occur closer to the wrong phase line, resulting in erroneous values for I_1 and I_2. By designing the system to maximize the spacing between the phase lines, the probability of these errors can be minimized.[14] The spacing between 2 phase lines, ρ, with integer phase corrections I_{11} and I_{12} for the first line and I_{21} and I_{22} for the second line, is given by

$$\rho = \frac{\left|\frac{\lambda_1}{\lambda_2}2\pi(I_{21}-I_{11})+2\pi(I_{12}-I_{22})\right|}{\sqrt{\left(\frac{\lambda_1}{\lambda_2}\right)^2+1}}. \tag{12}$$

The upper plot of Fig. 9 shows the minimum phase line spacing for varying values of λ_2 while λ_1 is held constant at 12.5 cm. The bottom plot shows the maximum values of I_1 and I_2 used to calculate the minimum phase spacing for $\theta_{max} = 80°$. Some of the discontinuities in the upper plot are caused by changes in the maximum values of I_1 and I_2 shown in the bottom plot. For some values of λ_2, the phase spacing is zero, indicating that some of the phase lines overlap, making it impossible to resolve phase ambiguities. Previous examples used $\lambda_2 = 15.625$ cm, which is indicated in Fig. 9 to be a local maximum, creating relatively wide phase-line spacings. The case of $\lambda_2 = 11.538$ cm, also marked in Fig. 9, is an example with relatively small phase spacing, resulting in the phase lines in Fig. 10.
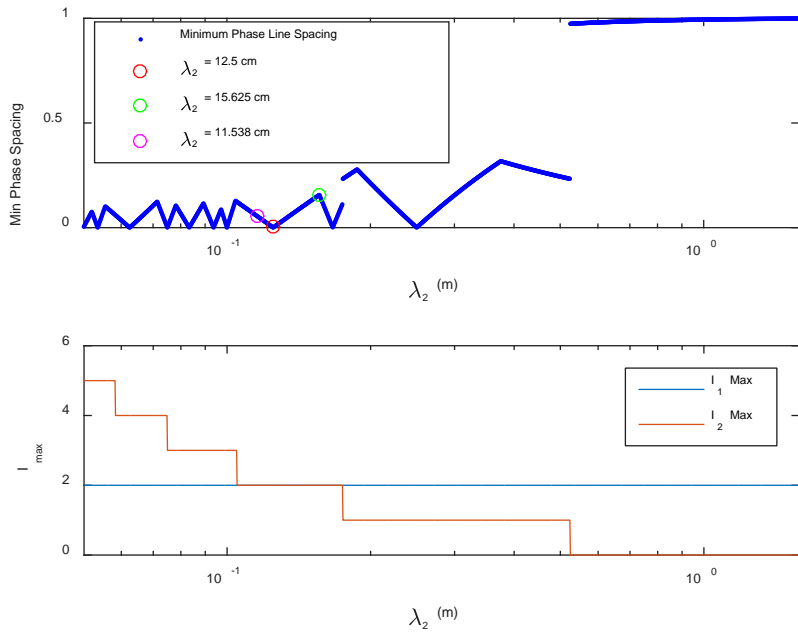
Fig. 9   Minimum phase-line spacing vs. wavelength (top) and the corresponding maximum integer ambiguity values (bottom)
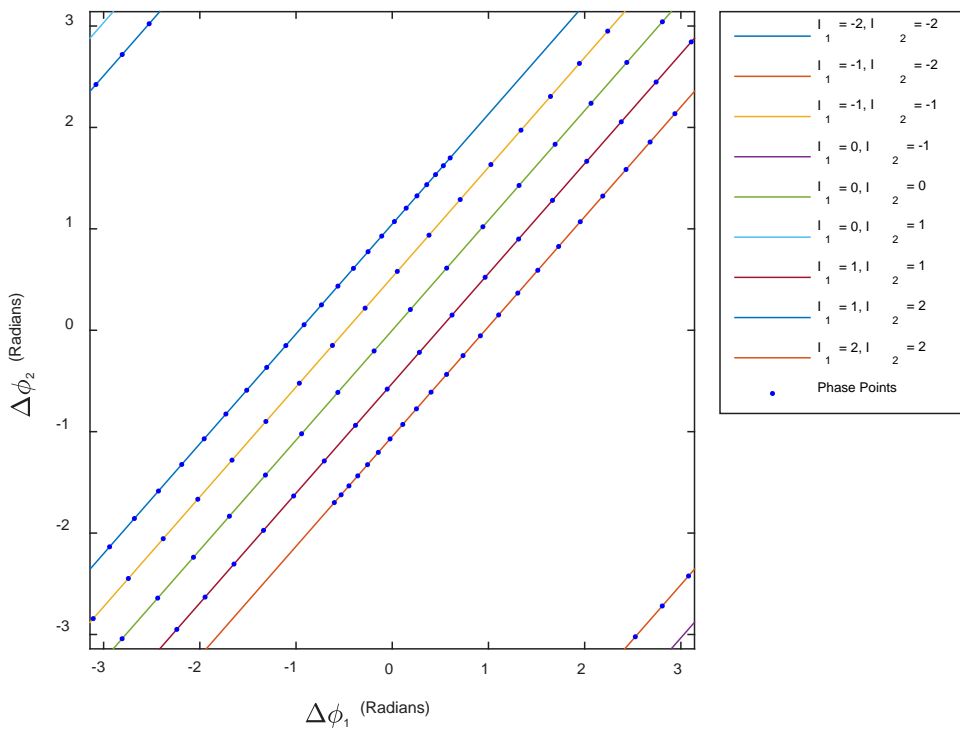
Fig. 10   Example of nonideal phase-line spacing

Although in many direction-finding applications the assumption that the distance to the radio source is much greater than d, in swarming scenarios it is possible that agents may be quite close to each other. Therefore, it is necessary to explore the accuracy of the previous assumption that the incoming radio signals to both antennas are parallel. Figure 11 shows the geometry of an RDF system where incoming RF signals are not assumed to be parallel. As in Fig. 1, A_1 and A_2 are the positions of the 2 antennas. θ is the AoA but is now measured from the midpoint between A_1 and A_2 labeled M. r_1, r_m, and r_2 are the distances from the RF source to A_1, M, and A_2, respectively. Using the law of cosines,

$$r_1 = \sqrt{r_m^2 + \frac{d^2}{4} - r_m d \cos\beta} \tag{13}$$

and

$$r_2 = \sqrt{r_m^2 + \frac{d^2}{4} - r_m d \cos\alpha}, \tag{14}$$

where $\beta = 90° - \theta$ and $\alpha = 90° + \theta$.
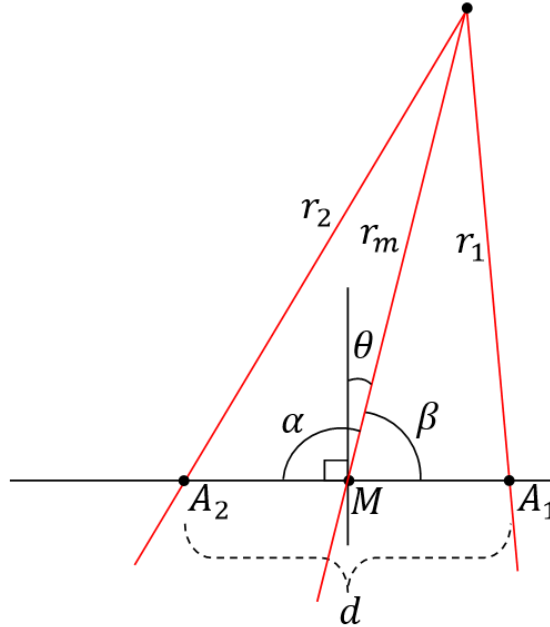
Fig. 11   AoA system with source close to antenna array

The top plot of Fig. 12 shows the error in the calculated AoA using the parallel assumption from Fig. compared with the more accurate geometry in Fig. 11 for $\lambda = 12.5$ cm, $d = \lambda$, and $r_m = 10$ m. The bottom logarithmic plot shows the maximum error versus the source range r_m for 3 different choices for antenna spacing d. At a distance of 0.5 m, even the worst case has an error of less than 1°, showing that even for relatively close distances the parallel assumption is very accurate.
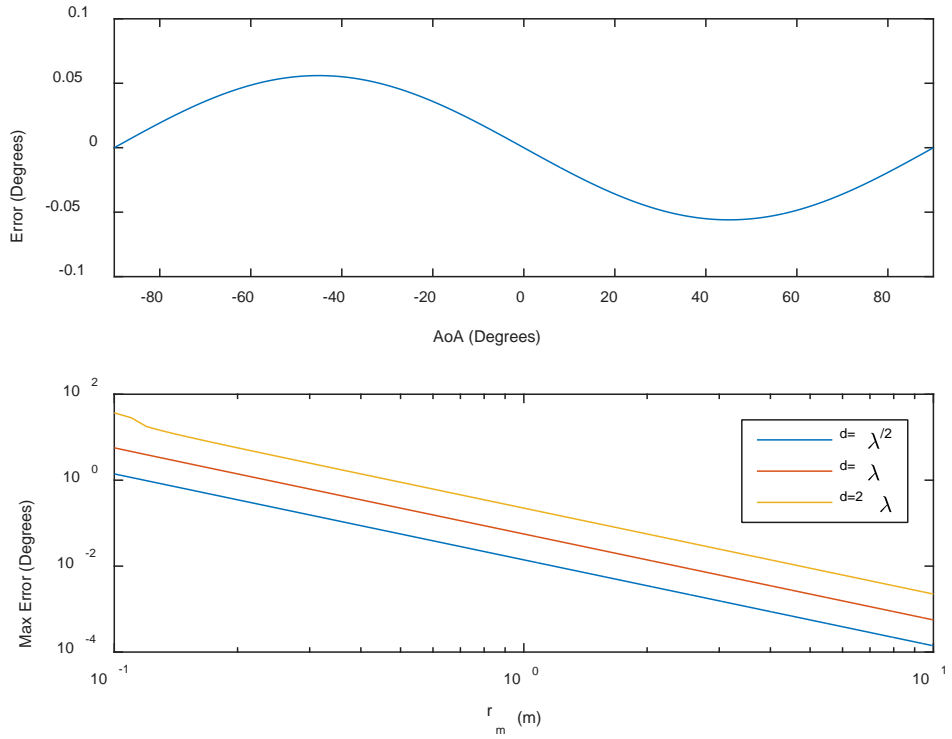
Fig. 12   AoA error of the parallel assumption for an example case (top) and the maximum error vs. r_m for 3 values of *d* (bottom)

3.   Experiment Setup

Now that RDF theory has been presented, a practical experiment to test the performance of a RDF system is described in the following. Figure 13 shows the experiment setup. An RF signal generator is used to produce the source signal, which is transmitted by a horn antenna in an anechoic chamber. The receiving antenna array and SDR are mounted on a rotary actuator. Figure 14 shows a picture of the antenna array mounted on the actuator in the anechoic chamber, and Fig. 15 shows a close-up of the antenna array. A PC controls the actuator to vary the AoA and records data from the SDR for RDF postprocessing. The SDR is discussed, followed by an overview of the control software.
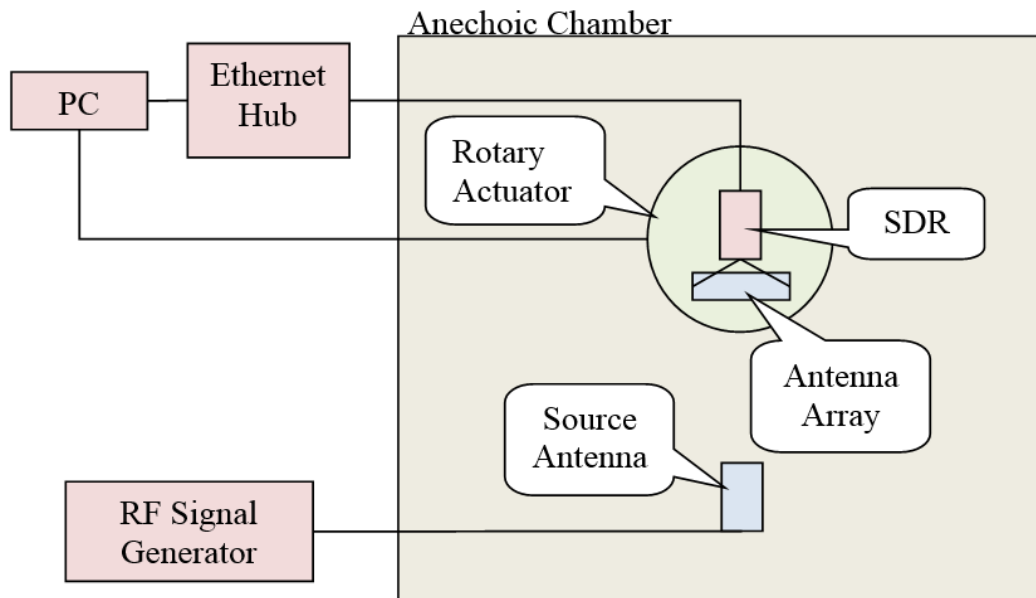
Fig. 13   RDF experiment setup
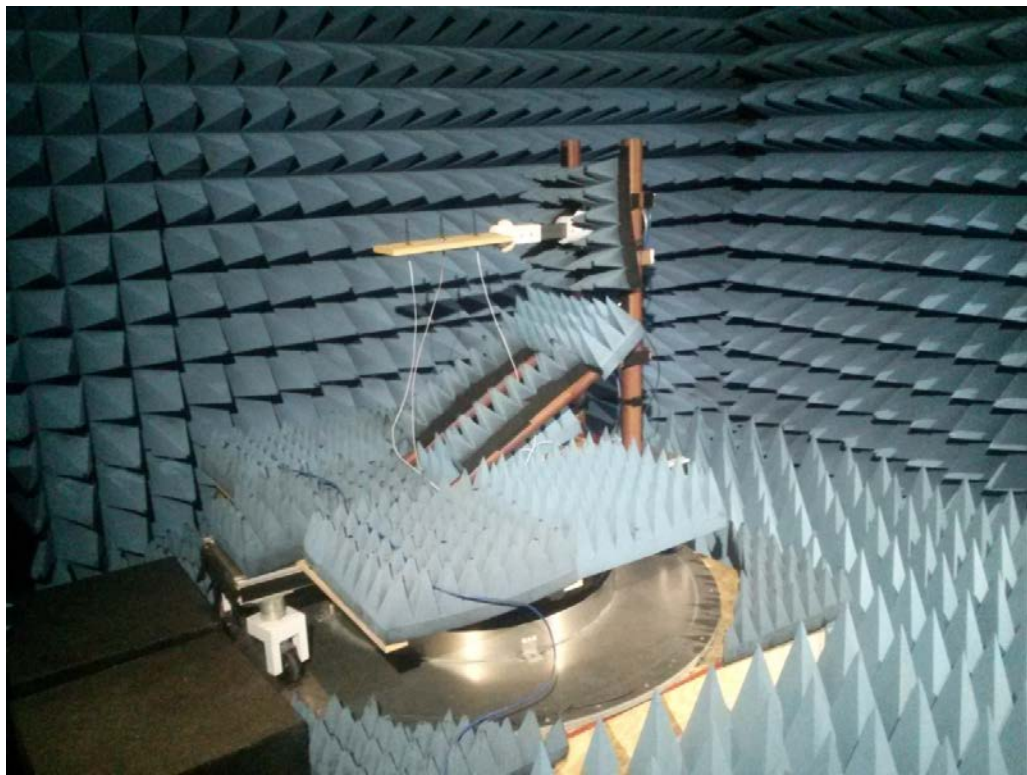
Fig. 14   Receiver setup in the anechoic chamber
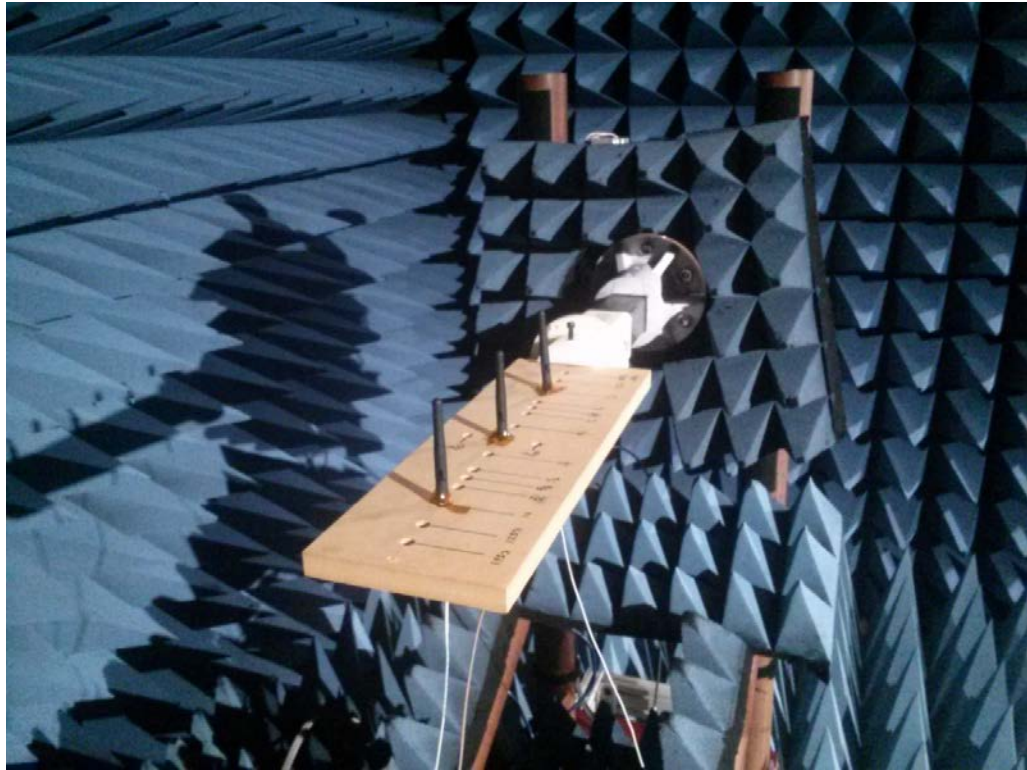
Fig. 15   Close-up of an example antenna array. The antenna in the middle is used for a calibration process described later.

SDRs are versatile platforms that are ideal for custom applications such as RDF. Whereas traditional radio systems are entirely implemented in hardware, SDRs digitize the RF signals and then process them in software. This makes it possible to directly determine the phase differences necessary for AoA determination. Building on ARL's previous experience with Universal Software Radio Peripheral (USRP) SDRs,[15,16] the USRP E310 shown in Fig. 16 was chosen for this application.[17] The E310 can act as a standalone Linux system with 2 receivers and 2 transmitters operating between 70 MHz and 6 GHz. Its small size and standalone operation make it a potential choice for a fielded UAV RDF system.

Fig. 16   USRP E310

Figure 17 shows a simplified block diagram of the E310.[17] Received RF signals travel through filter banks before entering the Analog Devices 9361 RF integrated circuit (RFIC). Inside the RFIC, the signal is amplified, Inphase/Quadrature (IQ) demodulated to an intermediate frequency, and digitally sampled. The samples are passed to the PL (programmable logic) on the Zynq integrated circuit, where they are DDC (digitally down converted) to baseband and decimated. The final IQ data is then passed to the Zynq PS (processing system) running OpenEmbedded Linux for further processing.
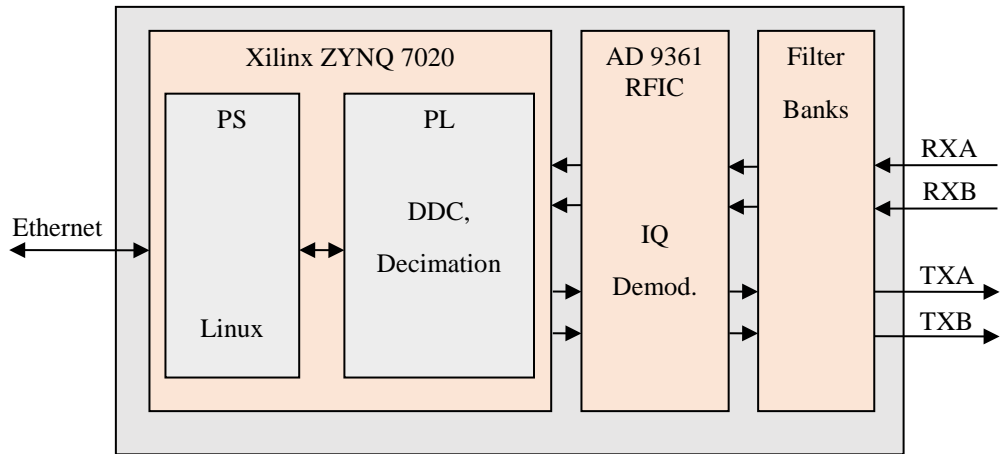
Fig. 17   USRP E310 block diagram

Although the IQ demodulation in the E310 involves a number of steps, the basic functionality is shown in Fig. 18.

14
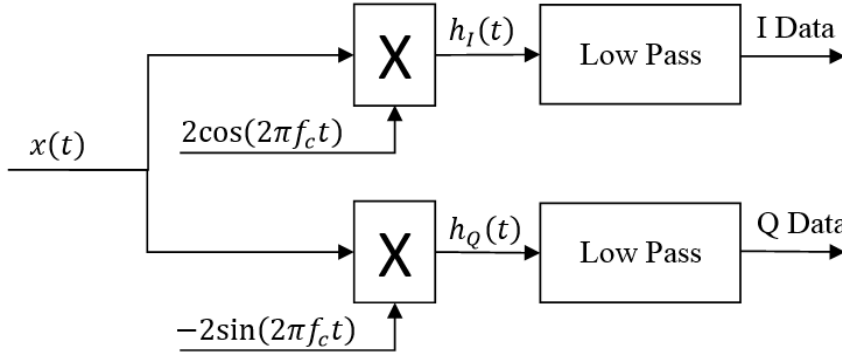
Fig. 18 IQ demodulator block diagram

The input RF signal $x(t)$ with carrier frequency f_c can be represented using IQ components as

$$x(t) = I(t)\cos(2\pi f_c t) - Q(t)\sin(2\pi f_c t). \tag{15}$$

Starting with the demodulation of the I data, Eq. 15 gives

$$h_I(t) = 2cos(2\pi f_c t)(I(t)\cos(2\pi f_c t) - Q(t)\sin(2\pi f_c t)). \tag{16}$$

Using the double angle formulas

$$\cos^2(\theta) = \frac{\cos(2\theta)+1}{2} \tag{17}$$

and

$$\sin(\theta)\cos(\theta) = \sin(2\theta), \tag{18}$$

$h_I(t)$ becomes

$$h_I(t) = I(t) + I(t)cos(4\pi f_c t) - Q(t)\sin(4\pi f_c t). \tag{19}$$

This leaves the baseband I data with additional signals at twice the carrier frequency. Filtering out these higher frequencies using a low-pass filter will restore the original I data. Similarly, for the Q data

$$h_Q(t) = -2sin(2\pi f_c t)(I(t)\cos(2\pi f_c t) - Q(t)\sin(2\pi f_c t)). \tag{20}$$

With the additional double angle formula

$$\sin^2(\theta) = \frac{1-\cos(2\theta)}{2}, \tag{21}$$

$h_Q(t)$ becomes

$$h_Q(t) = -I(t)sin(4\pi f_c t) + Q(t) - Q(t)\cos(4\pi f_c t). \tag{22}$$

Here the baseband Q data is left with additional high-frequency signals. Filtering out these high frequencies will restore the original Q data.

15

IQ demodulation can be applied to the signals in this RDF experiment. A single frequency, $f_c + f_b$, is used as the RF source. Through IQ demodulation, it is down-converted to a f_b baseband frequency while the phase information is preserved. To understand this process, we convert the source signal to the IQ format in Eq. 15. Let the source be represented as

$$x(t) = \cos(2\pi t(f_c + f_b)). \tag{23}$$

The received signals at antennas A_1 and A_2 are then

$$x_1(t) = \cos(2\pi t(f_c + f_b) + \phi_1) \tag{24}$$

and

$$x_2(t) = \cos(2\pi t(f_c + f_b) + \phi_2). \tag{25}$$

Using the cosine sum formula

$$\cos(\alpha + \beta) = \cos\alpha\cos\beta - \sin\alpha\sin\beta, \tag{26}$$

with $\alpha = 2\pi t f_b + \phi$ and $\beta = 2\pi t f_c$, Eqs. 24 and 25 can be written as

$$x_1(t) = \cos(2\pi t f_b + \phi_1)\cos(2\pi t f_c) - \sin(2\pi t f_b + \phi_1)\sin(2\pi t f_c) \tag{27}$$

and

$$x_2(t) = \cos(2\pi t f_b + \phi_2)\cos(2\pi t f_c) - \sin(2\pi t f_b + \phi_2)\sin(2\pi t f_c). \tag{28}$$

This is the IQ signal representation in Eq. 15, with $I(t) = \cos(2\pi t f_b + \phi)$ and $Q(t) = \sin(2\pi t f_b + \phi)$. The phase is then

$$\phi = \tan^{-1}\frac{Q(t)}{I(t)}. \tag{29}$$

Thus, the recovered IQ data preserves the phase information of the antenna signals and can be used to calculate the AoA.

To acquire the IQ data, the USRP E310 was programmed using GNU Radio[18] to configure its 2 receivers and send IQ data over user datagram protocol (UDP) to the control PC. The program, test_udp.py, is included in Appendix A. PuTTY,[19] an open-source terminal emulator on the control PC, was used to interface with the E310 and run the GNU Radio programs. A LabVIEW[20] program, shown in Fig. 19, was developed to receive, analyze, display, and save the IQ data over UDP from the E310. It also controlled the rotary actuator by executing commands through an emulated serial port. AoA experiments were automated by configuring the actuator to sequence through a series of angles while saving data from the E310. Although the LabVIEW program performed some basic processing during the experiments, the final analysis was performed on the recorded data using Matlab.[21]
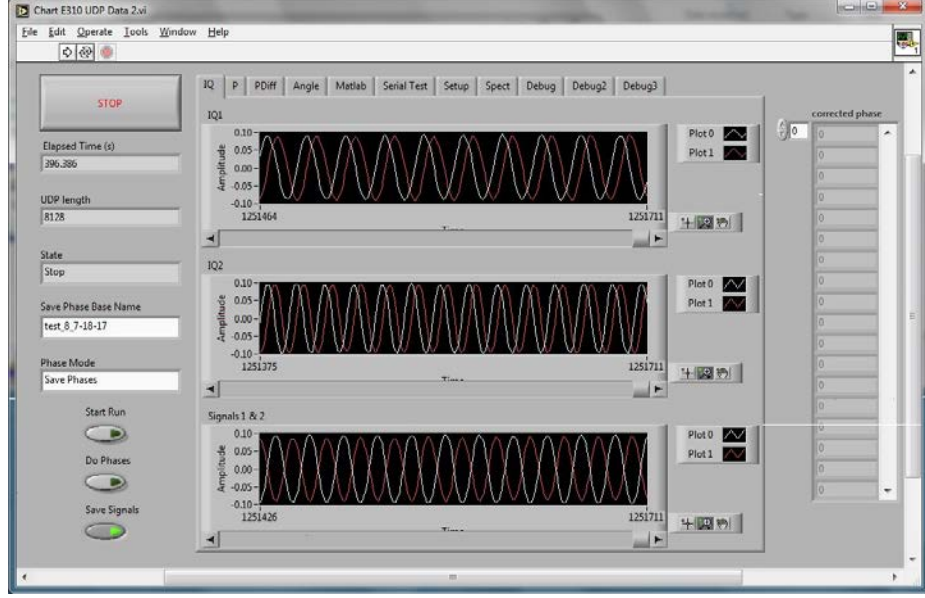
Fig. 19   Example screenshot of the LabVIEW program used to control the AoA experiment

4.   Experiment Results

Several experiments were performed to characterize the performance of this RDF system. The first was a high-resolution experiment using standard antenna spacing and power levels. The second tracked performance as the power level was decreased. The third experiment investigated the effect of varying the antenna spacing. The last experiment explored the feasibility of determining the SDR's unknown initial phase offset.

In the first experiment, 2 wavelengths were used to resolve phase ambiguities using the parameters listed in Table 1. Figure 20 shows example IQ data from the E310 for the 2 antennas at a single θ. Phases were extracted from the IQ data using Eq. 29 and shown in the top plot of Fig. 21. The middle plot shows the difference between the phases. Values outside of $\pm\pi$ occur due to phase rollovers. The bottom plot shows the corrected phase difference with all of the values wrapped inside of $\pm\pi$. The average of these phase differences is used for AoA calculations. At a modest sampling rate of 50 kHz, 27,433 samples were averaged over a period of 0.55 s to produce the final $\Delta\phi$ measurement for a given θ. Figure 22 shows the calculated $\Delta\phi$ measurements for $-45° \leq \theta \leq 45°$ with steps of $2.5°$, making a total of 36 $\Delta\phi$ samples for each wavelength. From these measurements, the phase points were plotted with their phase lines in Fig. 23. As in Fig. 6, these points are not positioned exactly on their phase lines, so the closest phase line was determined using Eq. 11 to resolve the integer ambiguities I_1 and I_2. These values are then used to unwrap $\Delta\phi_1$ and $\Delta\phi_2$ as shown in Fig. 24, and converted to the estimates of θ in

Fig. 25. The results were fairly accurate, with a maximum error of about 5°. More encouraging, however, are the results in Fig. 26 showing the repeatability of the same experiment performed 3 times, which had an average variance of 0.008° over the 3 trials of the 36 angle estimates in both λ_1 and λ_2. This indicates that significant increases in RDF accuracy may be achievable through calibration. It is difficult to determine the effectiveness of a calibrations procedure, however, until additional experiments are performed in more-realistic outdoor environments.

Table 1   Experiment 1 parameters

Parameter	Value	Definition
λ_1	12.5 cm	Wavelength 1
λ_2	15.625 cm	Wavelength 2
d	26.6 cm	Antenna spacing
G_{TX}	–3 dBm	Signal generator gain
G_{RX1}	70 dBm	Receiver 1 gain
G_{RX2}	70 dBm	Receiver 2 gain
f_s	50 kHz	Sampling frequency
f_b	1 kHz	Demodulated baseband frequency
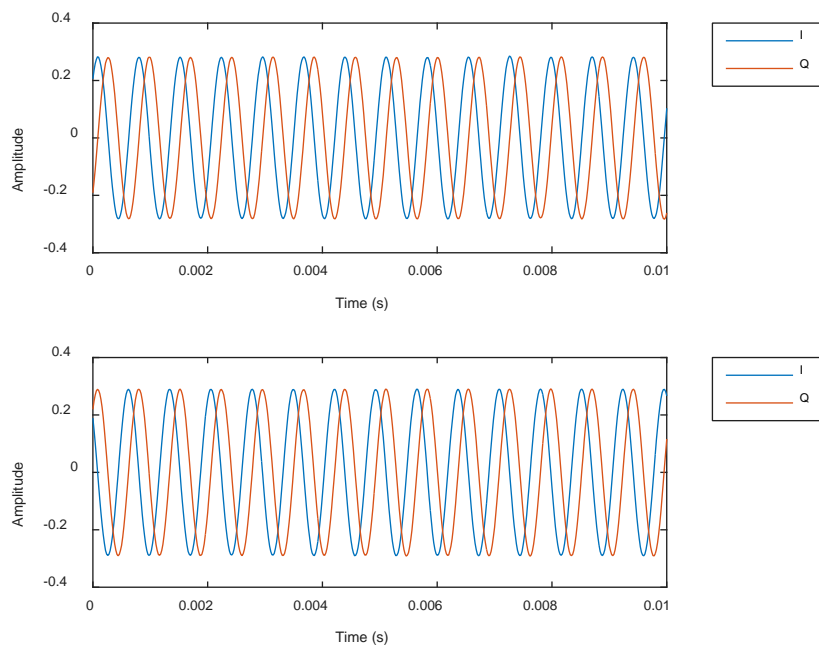
Fig. 20   IQ signals from antenna 1 (top) and antenna 2 (bottom)
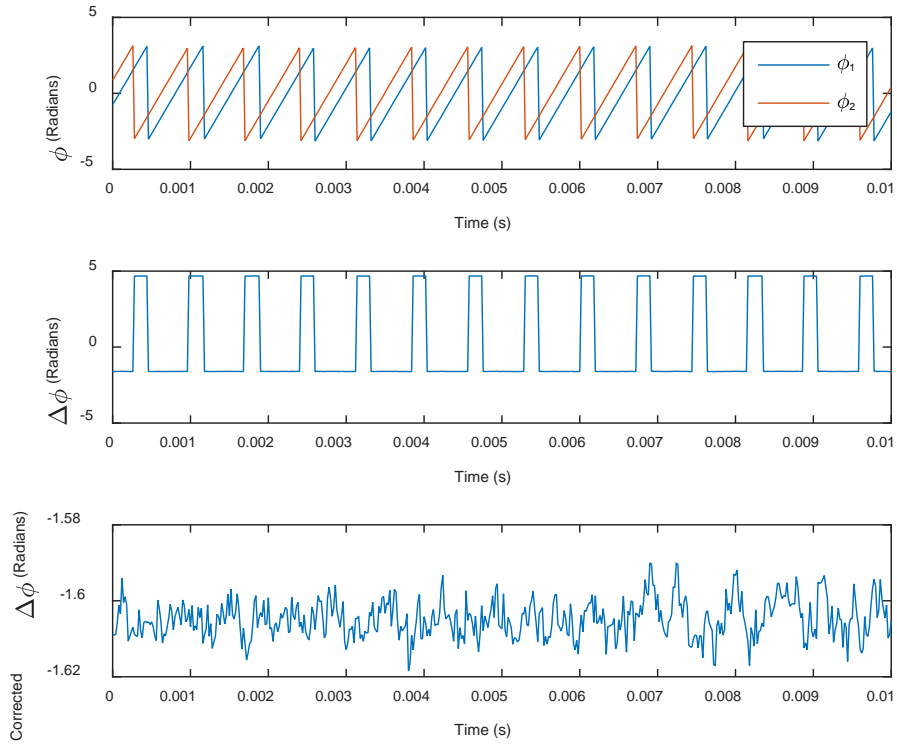
Fig. 21   Phase calculated from the IQ data (top), phase difference (middle), and corrected phase difference (bottom)
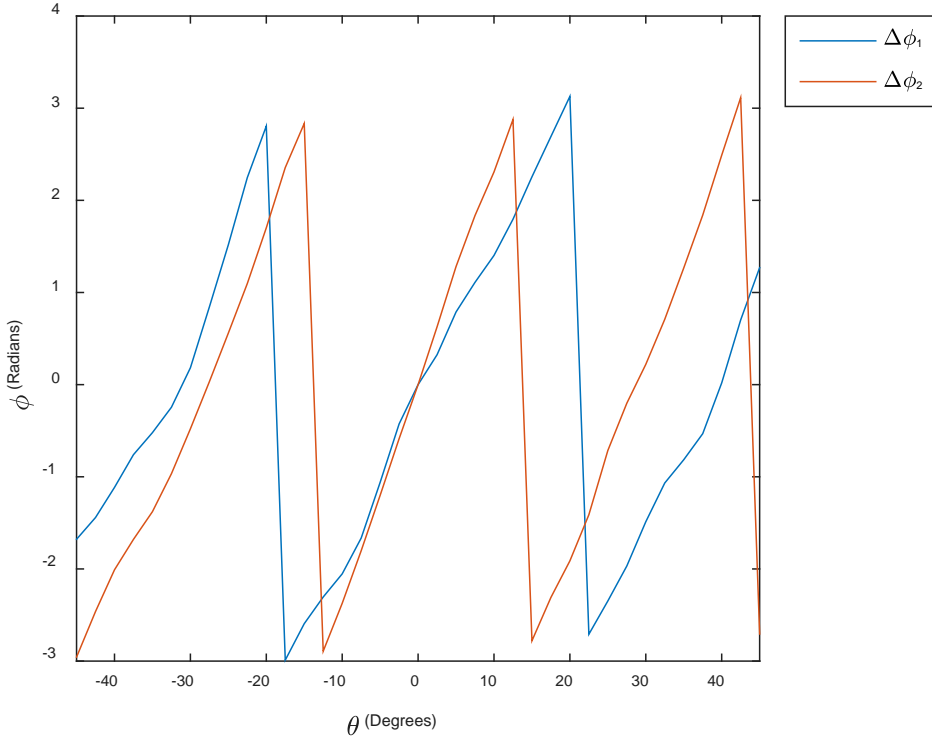
Fig. 22   Experimental phase measurements for 2 wavelengths
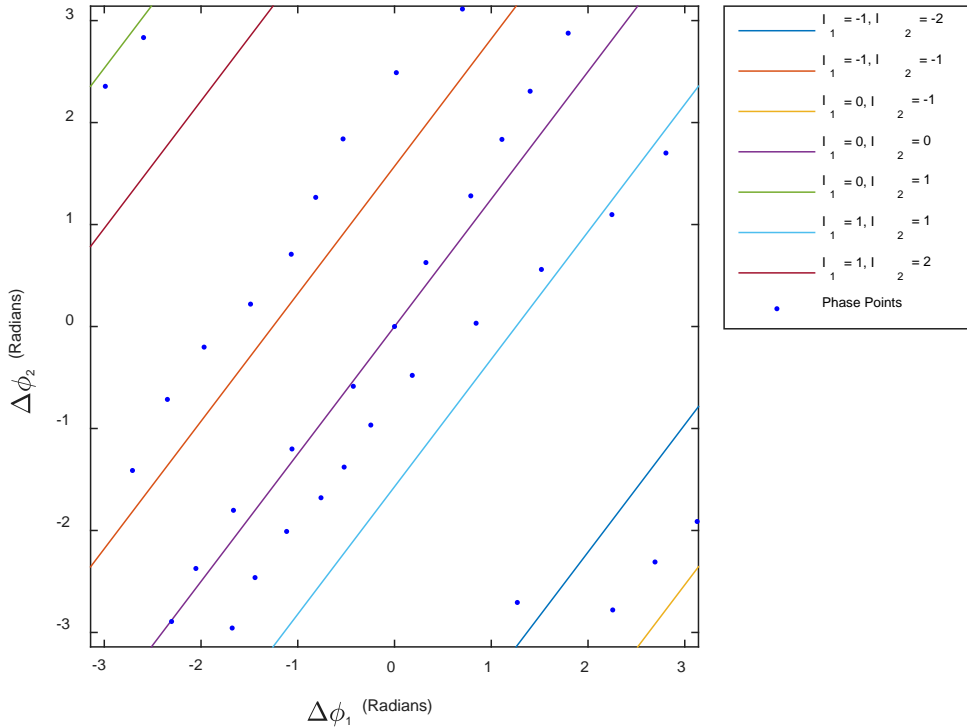
Fig. 23   Phase lines with experimental phase points
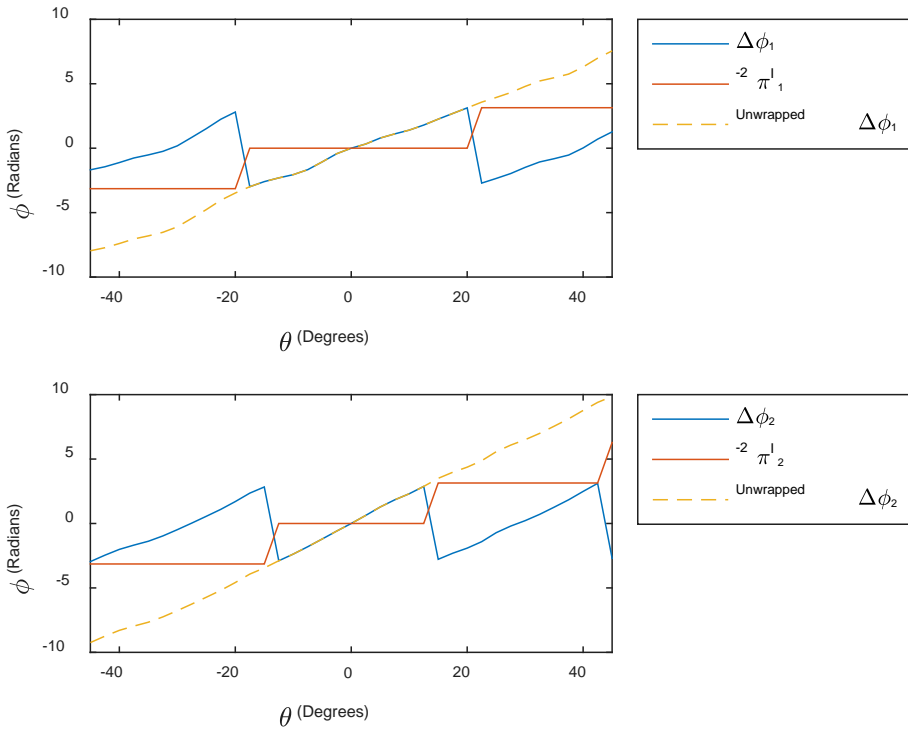
Fig. 24   Unwrapping experimental phase data from first wavelength (top) and second wavelength (bottom)
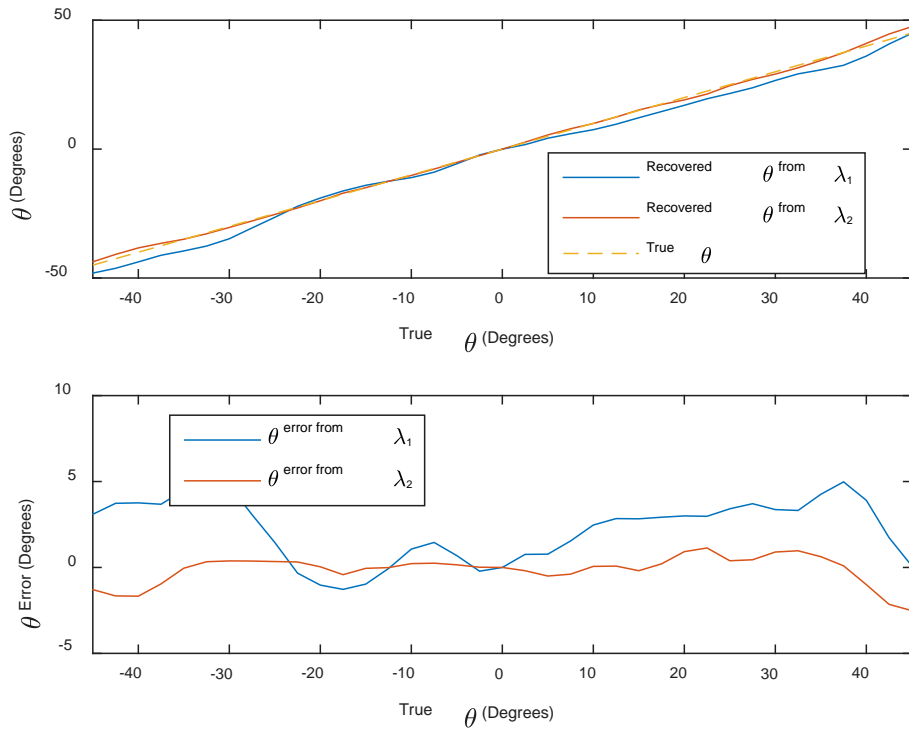
Fig. 25   AoA experiment results using 2 wavelengths (top) and AoA error (bottom)
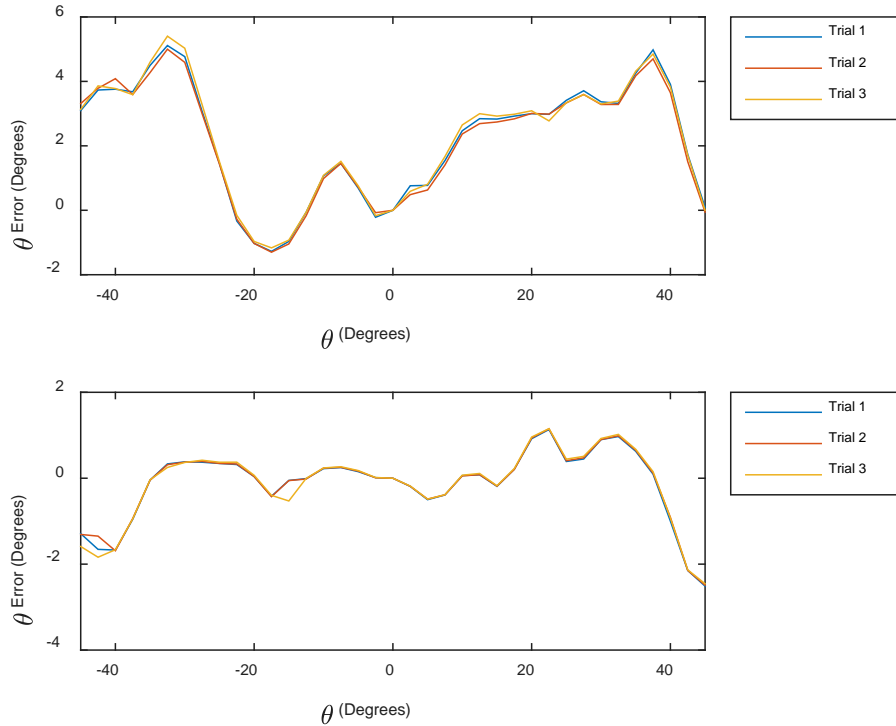
Fig. 26   Repeatability of experiment results using λ1 (top) and λ2 (bottom)

The experiment used the phase lines closest to the phase points to determine the values of I_1 and I_2, as shown in Fig. 23. In the following experiment, phase error caused some of the phase points to appear closer to the wrong phase lines, resulting in erroneous values of I_1 and I_2. Here, 12.5 cm was used for λ_1 and 14.58 cm for λ_2. Figure 27 shows the phase measurements and Fig. 28 shows the corresponding phase points, with the measurements that will result in erroneous integer ambiguity resolution marked. In Fig. 28 these erroneous points are closest to the phase line corresponding to $I_1 = -2$ and $I_2 = -1$. This leads to the unwrapped phase differences in Fig. 29, with the erroneous $-2\pi I$ correction factors indicated. This creates obvious phase difference errors in the unwrapped phases and angle errors in Fig. 30.
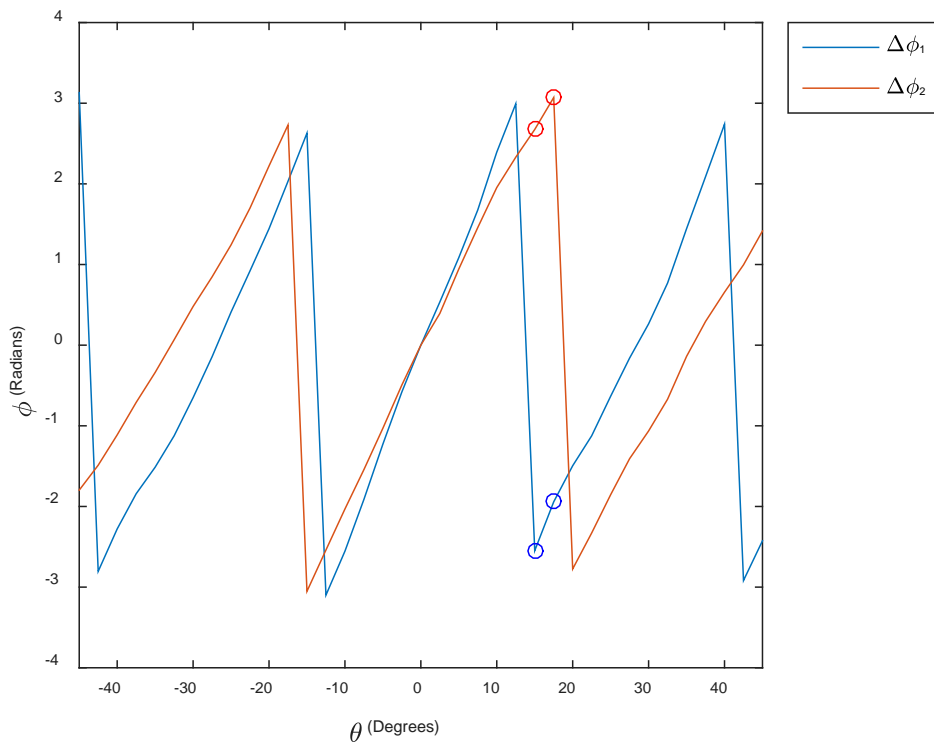
Fig. 27   Experiment phase measurements with erroneous points marked
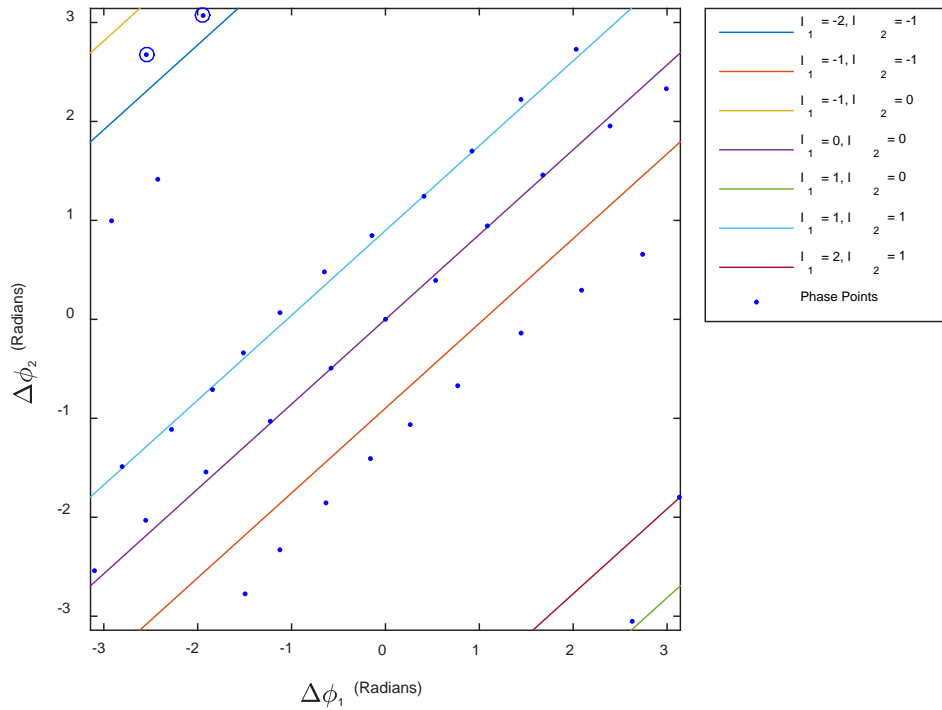
Fig. 28   Phase lines and phase points with erroneous points marked
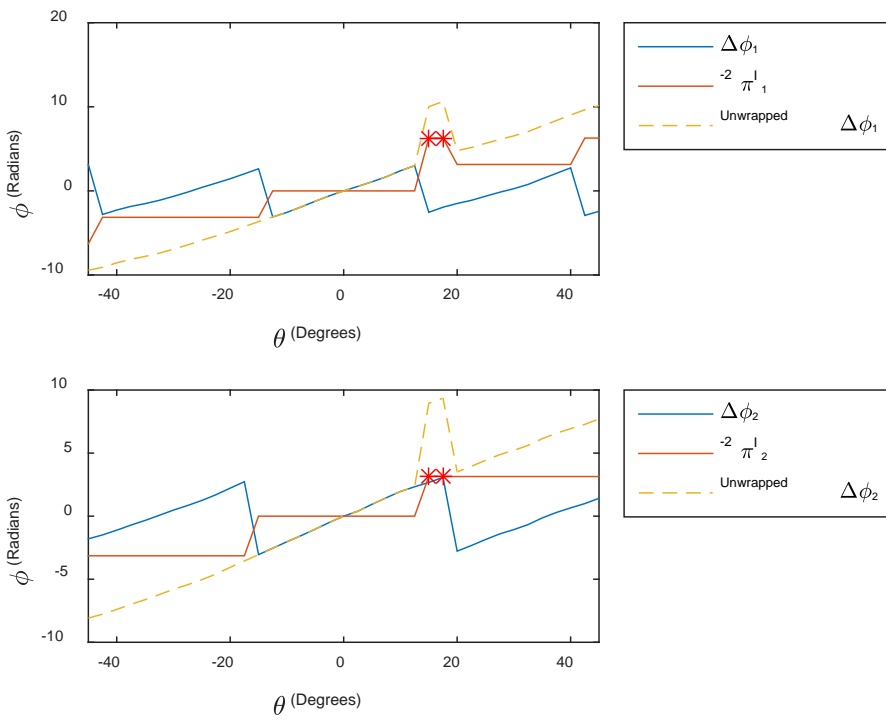
Fig. 29   Experimental results using 2 wavelengths with erroneous points marked
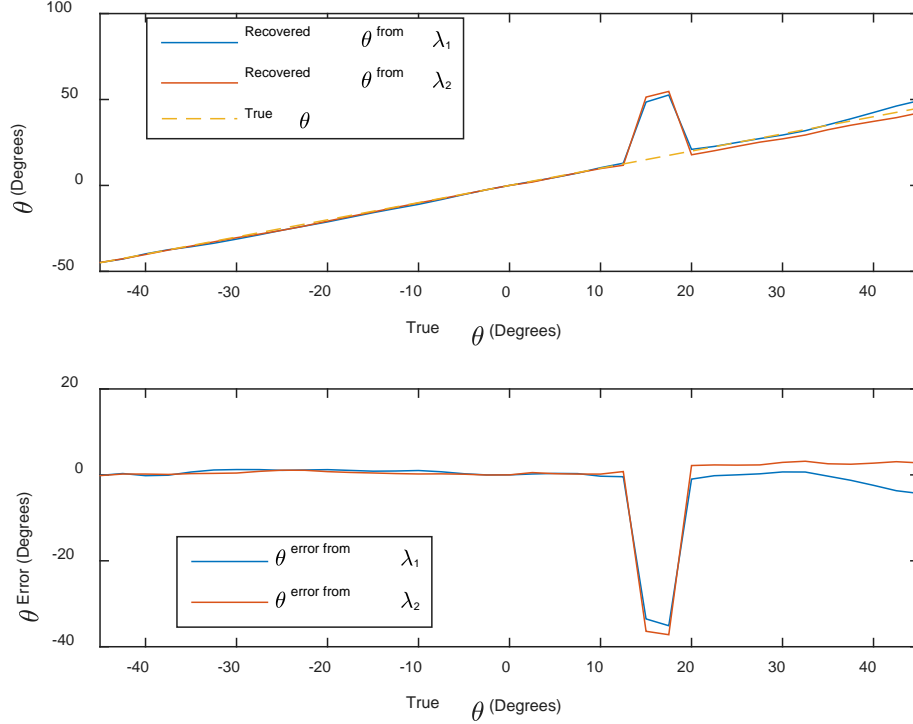
Fig. 30 **AoA experiment results using 2 wavelengths (top) and AoA error (bottom) with erroneous points included**

These types of errors can be corrected using a threshold for the maximum difference between one $\Delta\phi$ measurement and the next. In this case, the erroneous integer ambiguity resolution caused a jump in the unwrapped phase difference of about 2π. Using a threshold of $\Delta\phi_{max} = \pi$, if the difference between the previous $\Delta\phi$ measurement and current $\Delta\phi$ measurement is greater than $\Delta\phi_{max}$, the closest phase line is discarded, and the next closest phase line is used to resolve the integer ambiguity. This additional step results in the corrected unwrapped $\Delta\phi$ measurements in Fig. 31 and θ measurements in Fig. 32. In a field application, the higher the AoA sampling rate, the lower the difference between successive $\Delta\phi$ measurements. Thus, using high $\Delta\phi$ sampling rates could make this type of error correction very robust due to the tight bounds on $\Delta\phi_{max}$. It may also be possible to use inertial measurements from the transmitter and receiver agents to estimate the difference in $\Delta\phi$ between measurements, providing additional bounds on $\Delta\phi_{max}$.
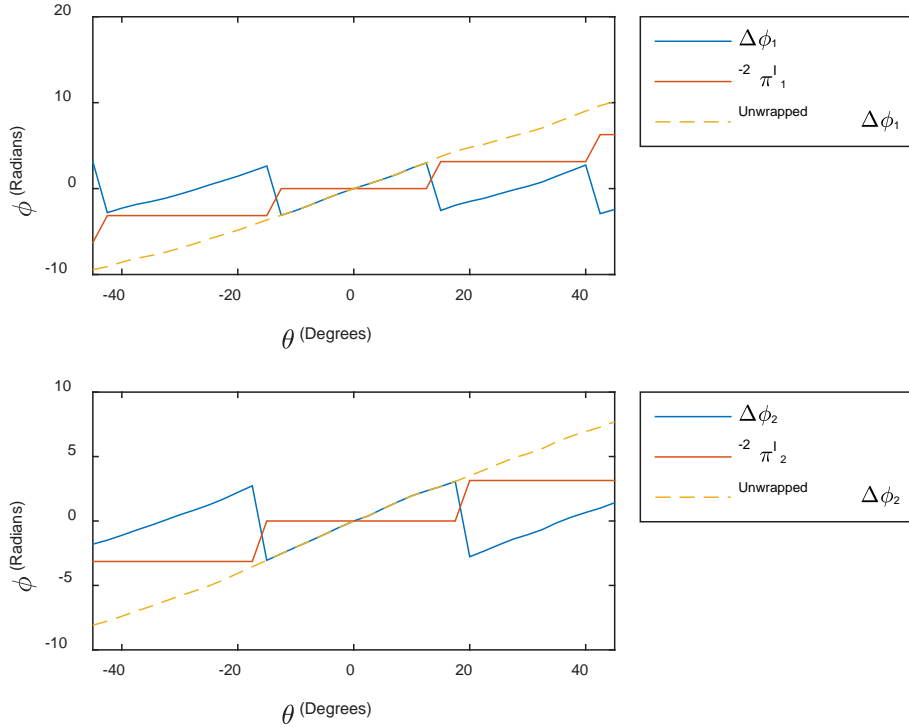
Fig. 31   Corrected phase unwrapping of first wavelength (top) and second wavelength (bottom)
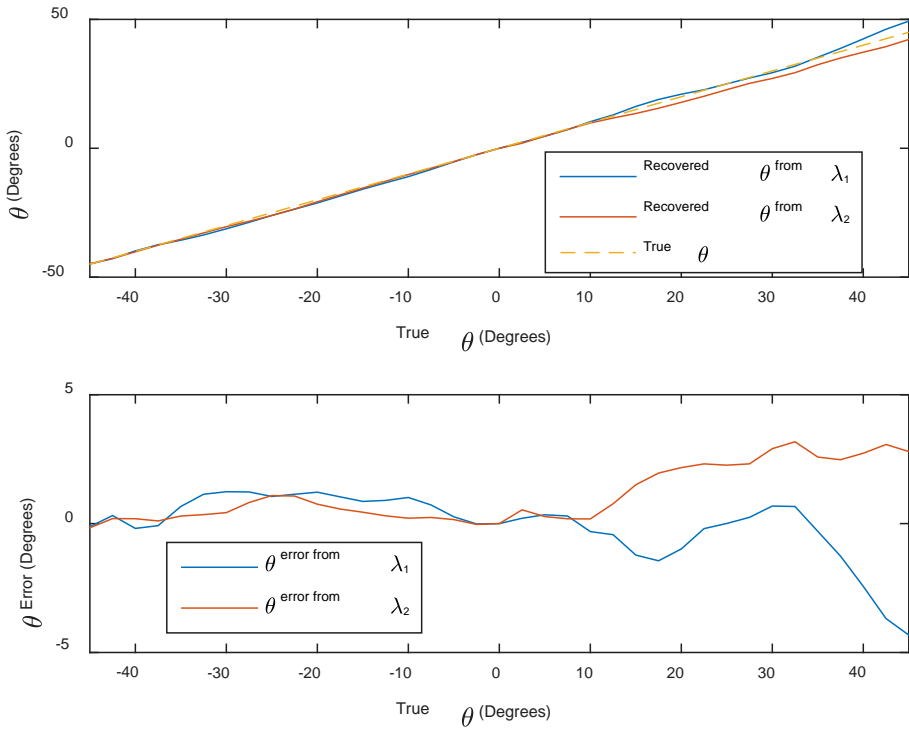
Fig. 32   Corrected AoA results (top) and AoA error (bottom) for 2 wavelengths

The next experiment determined the effects of transmit power on AoA error. Figures 33 and Fig. 34, corresponding to Figs. 20 and Fig. 21, show example noisy IQ and phase data. The spectrum of this noisy data is shown in the top plot of Fig. 35. Here, f_b is around 2 kHz and can be clearly seen as the frequency with the highest amplitude in the plot. Since the signal is so narrowband, a narrow-bandpass filter can be used to filter out most of the noise in the rest of the spectrum. The bottom plot of Fig. 35 shows the frequency response of a 16-pole Butterworth filter with a 200-Hz passband designed to filter the IQ data. The filtered IQ data are shown in Fig. 36 with corresponding phase signals in Fig. 37. Clearly, filtering has greatly improved the phase measurements. Using this filtering method, AoA experiments were performed at various transmit power levels. The top plot of Fig. 38 shows the AoA error of 4 experiments, 2 using a transmit power of –53 dBm and 2 using –73 dBm. Even at –53 dBm, the error is relatively low and appears to be repeatable. At –73 dBm, the error is significantly higher but still somewhat repeatable. It would be expected that as the noise increases, error caused by noise would overtake other error sources, resulting in random, nonrepeatable AoA errors. The plot, however, unexpectedly shows somewhat repeatable error even in the –73-dBm case. This interesting phenomenon requires further study. The bottom plot of Fig. 38 shows the average error over a range of transmit powers. Using information about the test setup, it is possible to convert this transmit power to an estimated distance.
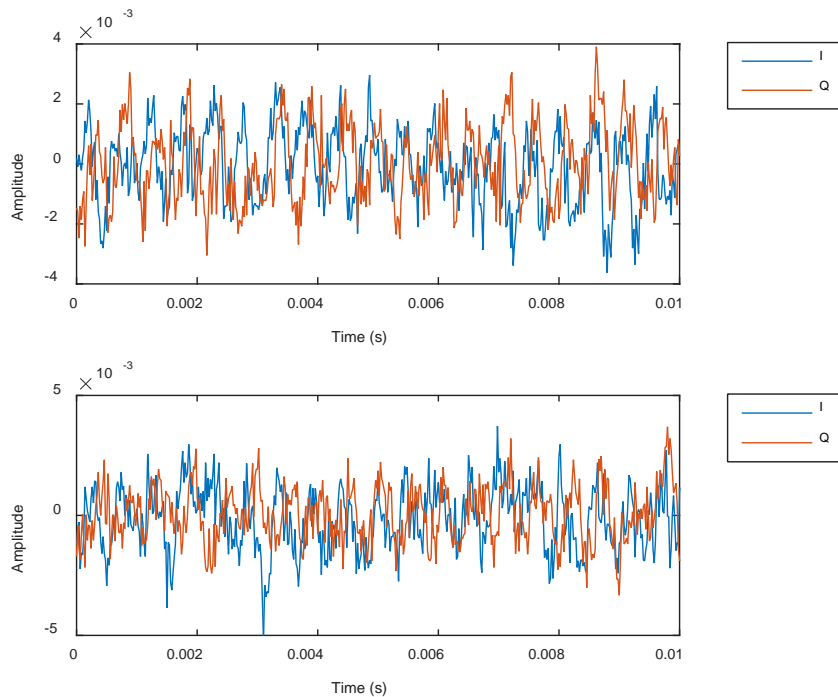
Fig. 33   IQ data from antenna 1 (top) and antenna 2 (bottom) for a transmit power of –53 dBm
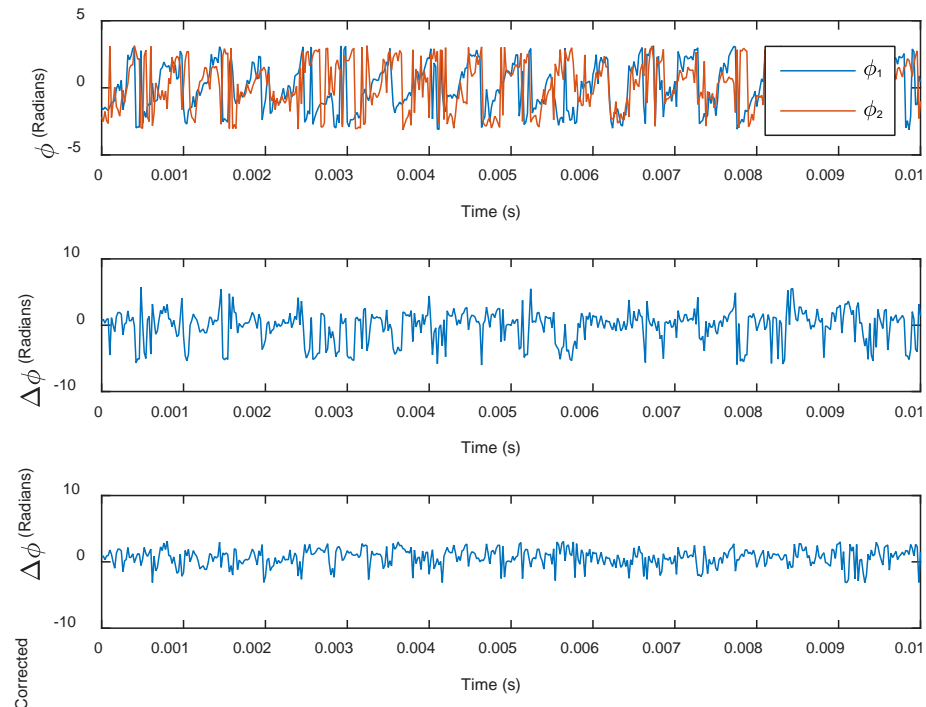
Fig. 34   Phase calculated from noisy IQ data (top), phase difference (middle), and corrected phase difference (bottom)
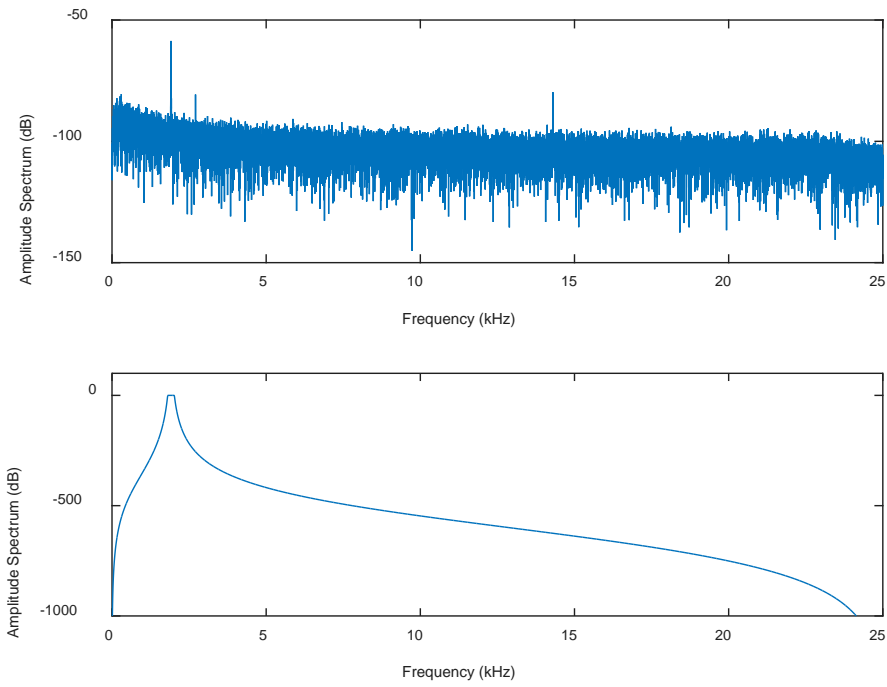
Fig. 35   Spectrum of example noisy IQ data (top) and frequency response of a filter designed to clean the IQ data (bottom)
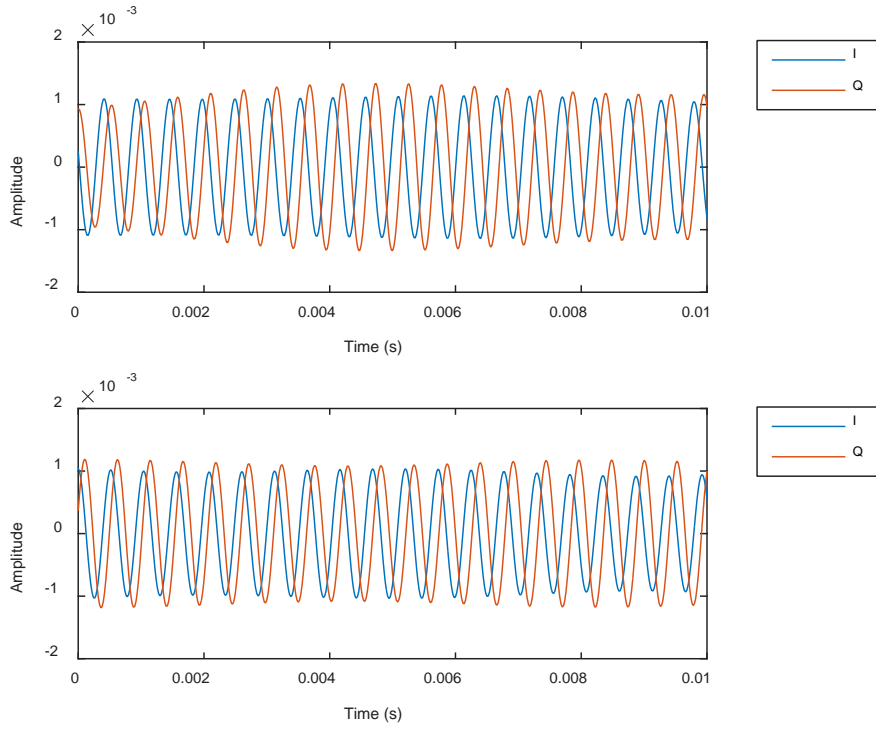
Fig. 36   Filtered IQ data from antenna 1 (top) and antenna 2 (bottom)
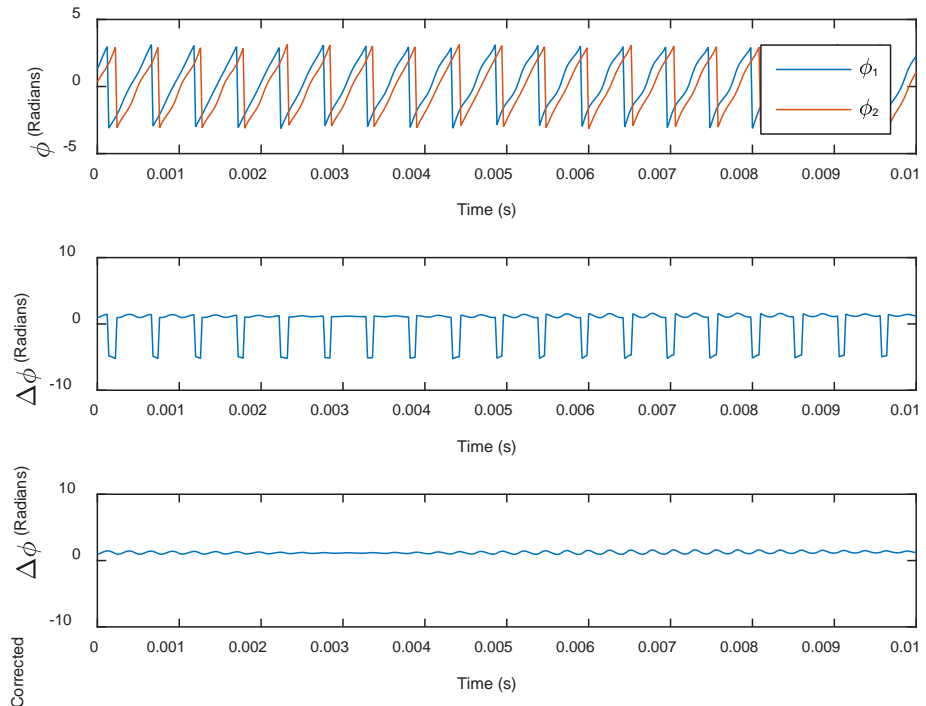
Fig. 37   Phase calculated from filtered IQ data (top), phase difference (middle), and corrected phase difference (bottom)
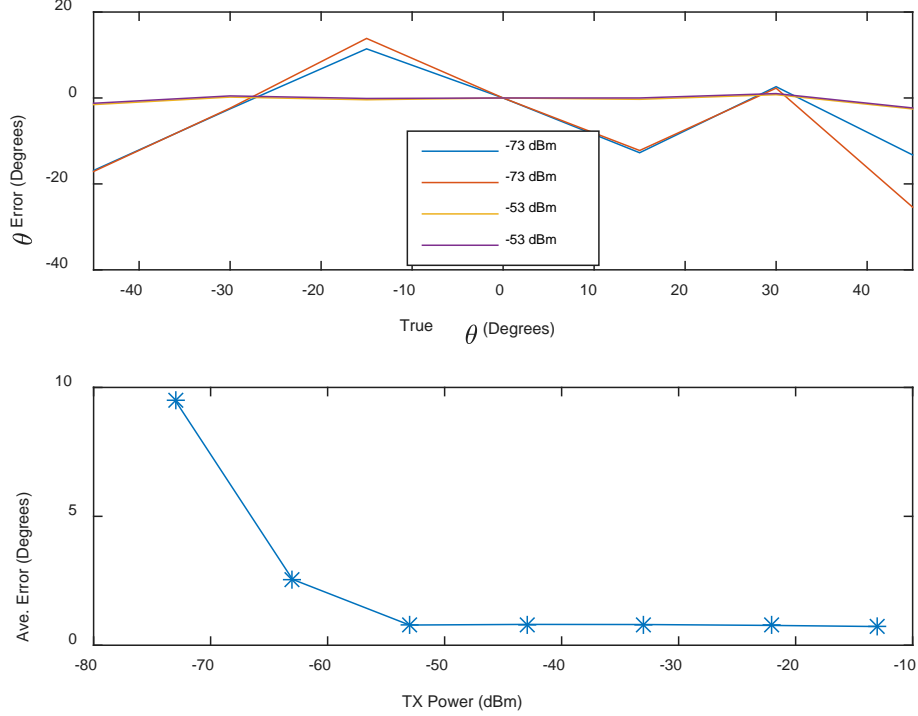
Fig. 38   Four AoA trials at 2 transmit powers (top) and average error vs. transmit power (bottom)

In the test setup, the transmit antenna gain was 9 dB, the cable loss from the signal generator to the antenna was 5 dB, and the distance from the transmit antenna to the receive antenna was 7.4 m. Using the equation for free-space path loss,

$$FSPL = 20 \log_{10} d + 20 \log_{10} f + 20 \log_{10} \frac{4\pi}{c}, \tag{30}$$

7.4 m corresponds to a path loss of 57.4 dB at 2.4 GHz. Including the other gains and losses gives a total loss to the receive antenna of –53.4 dB, resulting in a power at the receive antenna $P_{rx} = P_{tx} - 53.4$. In a field setting, a standard dipole transmit antenna with a gain of 2 dB, no cable loss, and a maximum transmit power of 10 dBm would give a total transmit power of 12 dBm. In this setting, the average error versus transmit power P_{tx} in Fig. 38 can be represented as distances using Eq. 30 as

$$d = 10^{(12-P_{tx}+53.4)/20+\log_{10} f+\log_{10}(4\pi/c)}, \tag{31}$$

shown in Fig. 39. The free-space path model is idealized, and might lead to overly optimistic range calculations, but in principle Fig. 39 shows that AoA measurements should work well even at great distances.
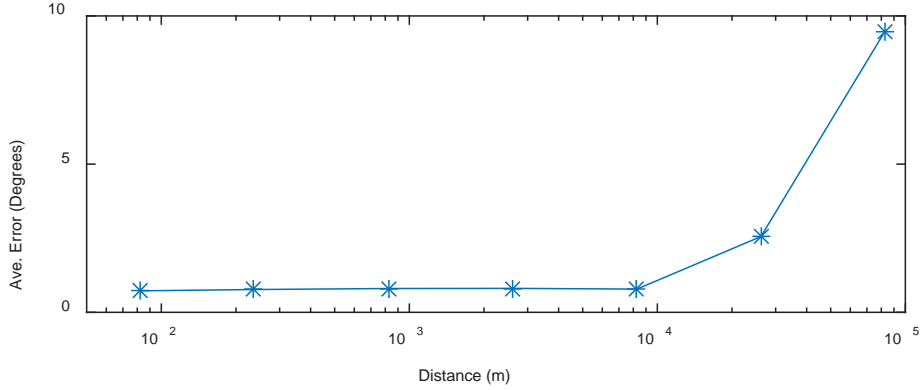
Fig. 39   Average AoA error vs. distance

The third experiment studied the effect of antenna spacing on AoA error. From Eq. 3, we see that as the antenna spacing increases, the AoA becomes less sensitive to variations in $\Delta\phi$. Therefore, greater antenna spacings should produce less AoA error. This theory is confirmed by the bottom plot of Fig. 40, showing AoA error decreasing as the antenna spacing increases. The top plot shows 4 trials, 2 at 6.65-cm spacing and 2 at 38.6 cm. While the smaller spacing produces more error, the error is repeatable. Thus, even constrained applications that must use smaller antenna spacings may be able to achieve accurate measurements if the error can be characterized and removed.
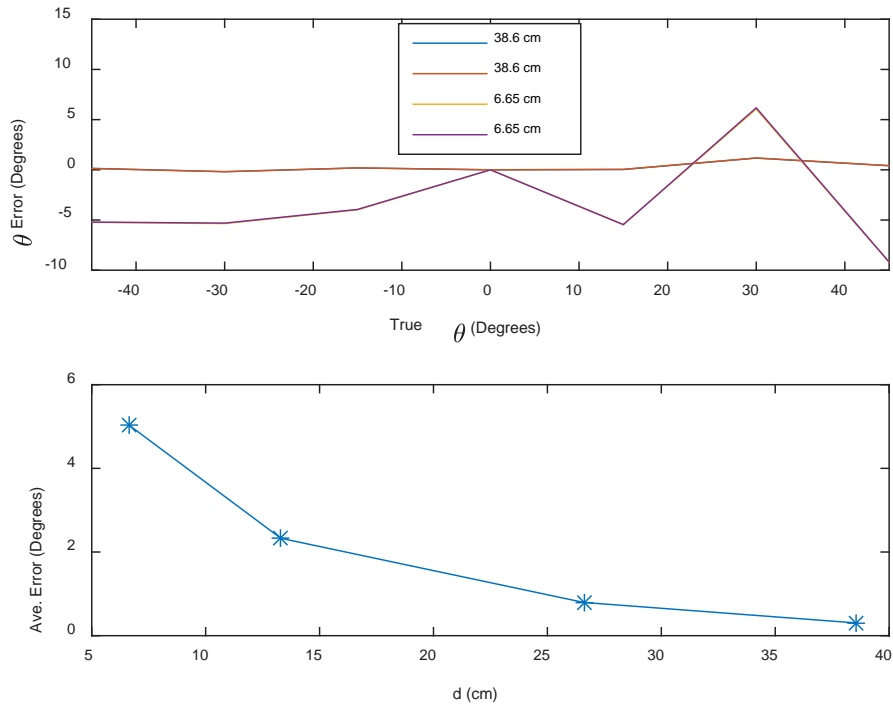
Fig. 40   Four AoA trials using 2 antenna spacings (top) and average error vs. antenna spacing (bottom)

In all of the experiments described, the unknown SDR phase bias, $\Delta\phi_{bias}$, was removed in postprocessing by subtracting the $\Delta\phi$ measurement at $\theta = 0°$, denoted as $\Delta\phi_0$, from all of the phase measurements. In practice, however, this bias information is unknown and requires a calibration method to be removed. One method is to transmit a signal at a known location to remove the bias. A third antenna was placed in the center of the antenna array, as shown in Fig. 15. A transmit port on the E310 was used to transmit from this third antenna and receive on the other 2 antennas using a calibration program, cal_test.py, included in Appendix B. This $\Delta\phi$ calibration measurement is denoted as $\Delta\phi_{cal}$. A normal measurement was then performed using the RF signal generator source at $\theta = 0°$ to find $\Delta\phi_0$, and $\Delta\phi_{bias}$ was calculated as

$$\Delta\phi_{bias} = \Delta\phi_0 - \Delta\phi_{cal}. \tag{32}$$

At a later date, new measurements $\Delta\phi'_0$ and $\Delta\phi'_{cal}$ were taken. Using $\Delta\phi_{bias}$ from Eq. 32, the new $\Delta\phi'_0$ measurement was estimated as

$$\Delta\tilde{\phi}'_0 = \Delta\phi_{bias} + \Delta\phi'_{cal}. \tag{33}$$

The error between $\Delta\tilde{\phi}'_0$ and $\Delta\phi'_0$ was 0.04 radians, corresponding to an AoA error of 0.17° using Eq. 2 and the standard parameters listed in Table 1. This demonstrates that $\Delta\phi_{bias}$ can be determined and removed with low error.

5. Conclusion

RDF is a promising technology for swarm localization. Initial testing in an anechoic chamber with an array of 2 antennas showed that results matched well with theoretical calculations over a range of antenna spacings. More importantly, abnormities were repeatable, showing that higher accuracy may be achieved through calibration. In this unique application where the swarm has control over the transmit frequency, multiple frequencies were used to resolve phase ambiguities. The use of a narrowband signals allowed filtering to remove noise and permitted extremely weak signals to be detected and processed. A calibration method to eliminate the unknown phase bias was demonstrated.

Future work will examine the use of additional antennas to allow for higher RDF resolution and the determination of elevation as well as azimuth angles. High-speed RF switches can be used to sample multiple antennas using one SDR receiver port,[22] allowing a single E310 with 2 receivers to support more than 2 antennas. Subspace methods lend themselves to analysis of the multiple signals that additional antennas will provide. These methods can be explored to increase RDF accuracy and determine the AoA of multiple sources simultaneously.[23]

Additionally, experiments in realistic environments should be performed and compared with results from the anechoic chamber. Further work should also consider the whole system, designing a scheme for the relative localization of an entire swarm based on RDF. This may include the use of RF sources for ranging and communications as well as RDF. Thus, RDF of the modulated signals used in communications should also be researched. System design will need to consider medium access issues and effects of noise and jamming. Localization should be modeled together with navigation to characterize swarm performance in relation to RDF design parameters. Although there is still much research to perform, this report has taken the first steps toward a practical RDF system for swarm localization.

# 6.	References

1.	Kurazume R, Nagata S, Hirose S. Cooperative positioning with multiple robots. Proceedings of the 1994 International Conference on Robotics and Automation; 1994.

2.	Bachrach A, Prentice S, He R, Roy N. RANGE – robust autonomous navigation in GPS-denied environments. J Field Robo. 2011;28.

3.	Parker R, Valaee S. Vehicular node localization using received-signal-strength indicator. IEEE Trans Vehicular Tech. 2007;56.

4.	Ryan A, Zennaro M, Howell A, Sengupta R, Hedrick JK. An overview of emerging results in cooperative UAV control. Presented at the 43rd IEEE Conference on Decision and Control; 2004 Dec 14–17; Nassau, Bahamas.

5.	Fresconi F, Fermen-Coker M. Delivery of modular lethality via a parent-child concept. Proceedings of the AIAA Atmospheric Flight Mechanics Conference; 2015 Feb. p. 2708.

6.	Read W. Review of conventional tactical radio direction finding systems. Ottawa (Ontario): Defence Research Establishment; 1989 May.

7.	Howeth LS. History of communications electronics in the United States Navy. Washington (DC): GPO; 1963.

8.	Wikipedia. Direction finding [accessed 2017 August 28]. https://en.wikipedia .org/wiki/Direction_finding.

9.	Pine K, Evans ME, Sammut K, He F. Radio direction finding for maritime search and rescue. Proceedings of the 2004 IEEE Control Conference: 2004 July 20. Vol. 2; p. 723–730.

10.	Hasch J, Topak E, Schnabel R, Zwick T, Weigel R, Waldschmidt C. Millimeter-wave technology for automotive radar sensors in the 77 GHz frequency band. IEEE Trans Micro T Tech. 2012;60(3):845–60.

11.	Bulusu N, Heidemann J, Estrin D. GPS-less low-cost outdoor localization for very small devices. IEEE personal communications. 2000;7(5):28–34.

12.	Appadwedula S, Keller CM. Direction-finding results for a vector sensor antenna on a small UAV. Proceedings of the 4th IEEE Workshop on Sensor Array and Multichannel Processing; 2006 Jul 12. p. 74–78.

13.	Jacobs E, Ralston EW. Ambiguity resolution in interferometry. IEEE Trans Aero E Sys. 1981(6):766–80.

14. Guerin D. Passive direction finding. Worcester (MA): Worcester Polytechnic Institute; 2012 Oct 10.

15. Don M. A low-cost software-defined telemetry receiver. Proceedings of the 51st International Telemetering Conference; 2015 Oct 26–29; Las Vegas, NV.

16. Don M. Advances in a low-cost software-defined telemetry system. Presented at the 53rd International Telemetering Conference Proceedings; 2017 Oct; Las Vegas, NV.

17. USRP E310 embedded software defined radio [accessed 2017 August 28]. www.ettus.com/content/files/USRP_E310_Datasheet.pdf.

18. GNU Radio, the free and open software eEcosystem [accessed 2017 August 28]. www.gnuradio.org.

19. PuTTY: a free SSH and Telnet client [accessed 2017 August 28]. www.putty.org.

20. National Instruments LabVIEW full development system [accessed 2017 August 28]. www.ni.com/en-us/shop/labview.html.

21. Matlab [accessed 2017 August 28]. www.mathworks.com.

22. Doi Y, Moriya H, Ichige K, Arai H, Hayashi T, Matsuno H, Nakano M. Low-cost antenna array via antenna switching for high resolution 2-D DOA estimation. Proceedings of the 2013 IEEE Workshop on InSignal Processing Systems (SiPS); 2013 Oct 16. p. 83–88.

23. Krim H, Viberg M. Two decades of array signal processing research: the parametric approach. IEEE Signal Processing. 1996;13(4):67–94.

Appendix A. GNU Radio Radio-Direction-Finding (RDF) Program

_____

This appendix appears in its original form, without editorial change.

```
#!/usr/bin/env python2
# -*- coding: utf-8 -*-
##################################################

from gnuradio import blocks
from gnuradio import eng_notation
from gnuradio import gr
from gnuradio import uhd
from gnuradio.eng_option import eng_option
from gnuradio.filter import firdes
from optparse import OptionParser
import time

class test_udp(gr.top_block):

    def __init__(self):
        gr.top_block.__init__(self, "test_udp")

        ##################################################
        # Blocks
        ##################################################
        self.uhd_usrp_source_0 = uhd.usrp_source(
            ",".join(("", "")),
                cpu_format="fc32",
                otw_format='sc16',
                channels=range(2),
            ),
        )
        self.uhd_usrp_source_0.set_samp_rate(50e3)
        self.uhd_usrp_source_0.set_center_freq(2400e6, 0)
        self.uhd_usrp_source_0.set_gain(70, 0)
        self.uhd_usrp_source_0.set_center_freq(2400e6, 1)
        self.uhd_usrp_source_0.set_gain(70, 1)
        self.blocks_udp_sink_0_0 = blocks.udp_sink(gr.sizeof_gr_complex*1,
'192.168.0.111', 15, 20000, True)
        self.blocks_udp_sink_0 = blocks.udp_sink(gr.sizeof_gr_complex*1,
'192.168.0.111', 14, 20000, True)

        ##################################################
        # Connections
```

```
        ##################################################
        self.connect((self.uhd_usrp_source_0, 0), (self.blocks_udp_sink_0, 0))
        self.connect((self.uhd_usrp_source_0, 1), (self.blocks_udp_sink_0_0, 0))


def main(top_block_cls=test_udp, options=None):

    tb = top_block_cls()
    tb.start()
    try:
        raw_input('Press Enter to quit: ')
    except EOFError:
        pass
    tb.stop()
    tb.wait()


if __name__ == '__main__':
    main()
```

INTENTIONALLY LEFT BLANK.

Appendix B. GNU Radio Calibration Program

```python
#!/usr/bin/env python2
# -*- coding: utf-8 -*-
##################################################

from gnuradio import analog
from gnuradio import blocks
from gnuradio import eng_notation
from gnuradio import gr
from gnuradio import uhd
from gnuradio.eng_option import eng_option
from gnuradio.filter import firdes
from optparse import OptionParser
import time

class test_udp(gr.top_block):

    def __init__(self):
        gr.top_block.__init__(self, "test_udp")

        ##################################################
        # Blocks
        ##################################################
        self.uhd_usrp_source_0 = uhd.usrp_source(
            ",".join(("", "")),
            uhd.stream_args(
                cpu_format="fc32",
                otw_format='sc16',
                channels=range(2),
            ),
        )
        self.uhd_usrp_source_0.set_samp_rate(50e3)
        self.uhd_usrp_source_0.set_center_freq(2400e6, 0)
        self.uhd_usrp_source_0.set_gain(70, 0)
        self.uhd_usrp_source_0.set_center_freq(2400e6, 1)
        self.uhd_usrp_source_0.set_gain(70, 1)
        self.blocks_udp_sink_0_0    =    blocks.udp_sink(gr.sizeof_gr_complex*1,
'192.168.0.111', 15, 20000, True)
        self.blocks_udp_sink_0    =    blocks.udp_sink(gr.sizeof_gr_complex*1,
'192.168.0.111', 14, 20000, True)
        self.uhd_usrp_sink_0 = uhd.usrp_sink(
```

```python
        ",".join((","")),
        uhd.stream_args(
            cpu_format="fc32",
            otw_format='sc16',
            channels=range(1),
        ),
    )
    self.uhd_usrp_sink_0.set_samp_rate(50e3)
    self.uhd_usrp_sink_0.set_center_freq(2400002000,0)
    self.uhd_usrp_sink_0.set_gain(70,0)
    self.analog_const_source_x_0             =             analog.sig_source_c(0,
analog.GR_CONST_WAVE, 0, 0, 0.7)

    ##################################################
    # Connections
    ##################################################
    self.connect((self.uhd_usrp_source_0, 0), (self.blocks_udp_sink_0, 0))
    self.connect((self.uhd_usrp_source_0, 1), (self.blocks_udp_sink_0_0, 0))
    self.connect((self.analog_const_source_x_0, 0), (self.uhd_usrp_sink_0, 0))
    #self.connect((self.analog_const_source_x_1, 0), (self.uhd_usrp_sink_0, 1))

def main(top_block_cls=test_udp, options=None):

    tb = top_block_cls()
    tb.start()
    try:
        raw_input('Press Enter to quit: ')
    except EOFError:
        pass
    tb.stop()
    tb.wait()

if __name__ == '__main__':
    main()
```

List of Symbols, Abbreviations, and Acronyms

AoA   angle of arrival

ARL   US Army Research Laboratory

DDC   digitally down converted

GPS   Global Positioning System

IQ   Inphase/Quadrature

PC   personal computer

PL   programmable logic

PS   processing system

RDF   radio direction finding

RF   radio frequency

RFIC   RF integrated circuit

SDR   software-defined radios

UAV   unmanned aerial vehicle

UDP   user datagram protocol

USRP   Universal Software Radio Peripheral

1 (PDF)	DEFENSE TECHNICAL INFORMATION CTR DTIC OCA
2 (PDF)	DIRECTOR US ARMY RESEARCH LAB RDRL CIO L IMAL HRA MAIL & RECORDS MGMT
1 (PDF)	GOVT PRINTG OFC A MALHOTRA

25
(PDF)
	DIR ARL
	RDRL WML F
	    B ALLIK
	    B J ACKER
	    T G BROWN
	    S BUGGS
	    E BUKOWSKI
	    J COLLINS
	    J CONDON
	    B DAVIS
	    M DON
	    D EVERSON
	    D GRZYBOWSKI
	    R HALL
	    J HALLAMEYER
	    M HAMAOUI
	    T HARKINS
	    M ILG
	    B KLINE
	    J MALEY
	    C MILLER
	    P MULLER
	    B NELSON
	    D PETRICK
	    K PUGH
	    N SCHOMER
	    B TOPPER

Approved for public release; distribution is unlimited.

43

INTENTIONALLY LEFT BLANK